

EVALUATION OF THERMAL MODELS ON
A MACHINING CENTER

By

CHRISTOPHER D. MIZE

A DISSERTATION PRESENTED TO THE GRADUATE SCHOOL
OF THE UNIVERSITY OF FLORIDA IN PARTIAL FULFILLMENT
OF THE REQUIREMENTS FOR THE DEGREE OF
DOCTOR OF PHILOSOPHY

UNIVERSITY OF FLORIDA

1998

ACKNOWLEDGMENTS

An undertaking of this scale requires the assistance of many people. I would like to thank my chairperson Dr. Scott Smith for his assistance and persistence for remaining on my committee after his departure to the University of North Carolina at Charlotte. I also thank the remaining members of my committee for their input and time spent reviewing this document. Special thanks go to Dr. John Ziegert for his availability to discuss the many topics encountered in this research.

I would like to thank Mike Niemotka at Tetra Precision for his invaluable assistance programing the machine tool and helping with the measurements. Thanks go to Tony Schmitz in the Machine Tool Research Center for writing the CMM program and providing his simulation software for the tool dynamics. I would also like to thank Narayan Srinivasa for providing the neural network algorithm and his discussions about the network.

Thanks go to the personnel at Cincinnati Milacron for providing the necessary support for the special software required for compensation, and to Joe Godschalk and Joan Staubach for programming the compensation algorithm in the controller.

I would also like to thank the USAF, without whose funding this research would not have been possible.

TABLE OF CONTENTS

ACKNOWLEDGMENTS	ii
Abstract	vi
CHAPTER 1	
INTRODUCTION	1
Precalibrated Compensation	7
Research Objectives	8
CHAPTER 2	
LITERATURE REVIEW	12
Background	12
Geometric Compensation	12
Thermal Modeling and Compensation	15
Motivation for the Research	22
Scope of the Research	23
CHAPTER 3	
GEOMETRIC MODEL	25
Geometric Compensation	25
Kinematic Model for the Machining Center	27
Implementation in the Controller	32
CHAPTER 4	
THERMAL ERROR MODELS	34
Introduction	34
First Order Thermal Model	35
Implementation of the Model	36
Thermal Drift	37
The Neural Network Model	38
Incorporation of the Network in the Model	41
Implementation on the Machine	44
Thermal Sensor Placement	49

CHAPTER 5

MEASUREMENT AND MACHINING PROCEDURES	52
Geometric Error Measurement with the Laser Ball Bar	52
Data Collection Procedure	53
Data Collection for Model Verification	58
Body Diagonal Measurement Procedure	60
B5.54 Part Machining Procedures	60

CHAPTER 6

TEST RESULTS	64
Model Evaluations	64
Model Stability Evaluation	64
Diagonal Measurement Evaluation of the Models	69
Machine Part Evaluation	74

CHAPTER 7

CONCLUSIONS AND RECOMMENDATIONS	81
Success of Implementing Fuzzy ART-MAP on a Milling Machine	81
Geometric vs. Thermal Modeling	87
Deterministic vs. Non-deterministic Modeling	87
Training with Machining vs. Non-machining	89
Metal Removal Testing vs. Non-machining Testing	91
Surface Distance Error	92
Future Work	93

APPENDIX A

THE LASER BALL BAR	95
Background	95
The Instrument	96
Trilateration with the LBB	98
Determining LBB to Machine Coordinate Transformation	102
Parametric Error Reduction from Coordinate Data	104
Coordinate Error Sensitivity to Tetrahedron Geometry	105
Instrument Accuracy	108
Parametrics from Six Measurements	109

APPENDIX B

KINEMATIC MODEL IN CONTROLLER	112
-------------------------------	-----

APPENDIX C

PARAMETRIC ERROR MEASUREMENT DATA	117
-----------------------------------	-----

LIST OF REFERENCES	142
BIOGRAPHICAL SKETCH	147

Abstract of Dissertation Presented to the Graduate School
of the University of Florida in Partial Fulfillment of the
Requirements for the Degree of Doctor of Philosophy

EVALUATION OF THERMAL MODELS ON A
MACHINING CENTER

By

Christopher D. Mize

August 1998

Chairperson: Kevin S. Smith

Major Department: Mechanical Engineering

Machine tool positioning accuracy varies with the thermal state of the machine. As electrical energy is input into the servomotors, hydraulic pumps, and other machine systems, energy is transferred into the part, atmosphere, and most importantly the machine's structure. This transfer of energy throughout the machine results in temperature changes and thus structural deformations that change the machine's accuracy. In order to mitigate these detrimental accuracy variations, models have been employed that try to predict and correct for these variations based on discrete temperature readings from the machine. In this study three thermal models and one geometric model are evaluated by comparing their accuracy improvement on a Cincinnati Milacron Maxim 500 machining center. One thermal model is the simple geometric model with first order correction of the scale errors. The two remaining thermal models utilize a new implementation of a

neural network. One of the neural network models is trained from error measurements taken as the thermal state is varied with non-machining actuation, while the other utilizes actual machining. The laser ball bar is utilized to collect the training data for the models in a timely manner and to allow machining between measurements. The models are evaluated by measuring body diagonals with the laser ball bar and by comparing the accuracy of machined parts at different thermal states of the machine.

The body diagonal and part machining tests reveal that the thermal models are capable of 2-4X error reduction at several thermal states. The completely deterministic first order thermal model performed as well or better than the neural network models. Durability tests showed that the models were capable of error reduction over a 9 month period. No clear preference was found for training with or without machining, rather the use of coolant appeared to be a more important factor. Thermal compensation is a viable technique that should be embraced by industry.

CHAPTER 1 INTRODUCTION

Machine tools, assembly robots, and computer controlled positioning machines in general, have as their primary function to place an end effector relative to a work piece according to a controller's commanded position and orientation. In machine tools, this is manifested in the machine's ability to position the cutting tool relative to the part raw material. A machined part's accuracy is directly, one to one, dependent on this positioning capability. Other factors such as tool wear and dynamic effects (chatter) can also contribute, but unlike positioning error, their effects can be mitigated by proper planning at the time of production.

The accuracy with which positioning can be accomplished depends on many factors: accuracy of the axis feedback sensors, Abbe' effects, thermal stability, structural integrity, and dynamic stability, to name a few. Much effort has been spent in this century on improving machine tool accuracy, and understandably so, since machine tools are important to a nation's economy. They are a critical early link in a chain that has at one end a nation's natural resources and at the other its salable products. In 1991, the machining processes of turning, milling, drilling, and grinding, accounted for approximately \$115 billion annually in the U.S. discrete part industry, or about 2% of the GDP [Soons, 1995].

To reduce a machine's errors it is best to understand their source first. This can be accomplished by examining the individual systems making up the machine and how their non-ideal behavior effects part accuracy. A modern machine tool is comprised of a control system (digital computer), an actuation system (rotary or linear servomotors), a feedback system (linear or rotary encoders), a cutting system (spindle motor, and cutting tools), a part fixturing system (pallet or chuck), and a mechanical system (prismatic and rotary joints). Each of these systems can contribute to a machined part's inaccuracies.

Traditional machine tools achieve multi-degree positioning through a chain of prismatic and rotary joints combined in series, with the cutting tool at one end of the chain and the work piece at the other. Each joint is intended to provide a single degree of freedom. Recently machine tools have been developed that are based on parallel kinematic structures [Aronson, 1996, 1997]. While promising, these machines are still in the developmental phase. The focus of this research will be upon the industry dominant serial link machine.

Since direct volumetric positioning feedback between the cutting tool and the work table has not been perfected, machine tools rely upon position feedback from each joint for determining tool placement relative to the work table. This arrangement requires, infinitely stiff components, a perfect control system, perfect scales, a single degree of freedom at each joint, and isothermal behavior to achieve perfect positioning. Unfortunately this ideal scenario is not achievable. Errors are correspondingly classified into four major categories: control, elastic, geometric, and thermal.

Elastic deformations can result from cutting load induced deflections in the tool and machine structure as well as dynamic effects such as vibration (chatter). Quasi-static deflections in the structure caused by cutting forces and gravity can be reliably predicted through finite element modeling and adequately minimized by proper stiffening at the design stage. Elastic deformations caused by vibrations in the tool and spindle can be significant, but their discussion is beyond the scope of this research and necessary precautions can be taken to avoid their domain of existence. The control system can also be reliably modeled and optimized, minimizing this source of error. Geometric and thermal errors have reached a cost/design tradeoff limit that leaves them as the largest error contributors [Venugopal and Barash, 1986; Hocken, 1980; Bryan, 1990]. The geometric errors are limited by the precision and assembly of the machine's components. Cost to reduce these errors at the manufacturing stage can rise exponentially. Thermal errors, like elastic errors, can be reasonably modeled; however, they are not as easily mitigated at the design stage because the unavoidable heat sources can not be sufficiently insulated from the machine structure. The geometric and thermal errors remain as the primary obstacle to improved accuracy in machining and are the focus of this research.

Geometric errors can be attributed to the mechanical component inaccuracies that result in unwanted motions at each joint. Each joint is intended to have a single degree of freedom, but in reality has six degrees of error motion. For prismatic joints there is an intended displacement freedom which can be in error, two straightness errors perpendicular to the displacement, and three angular motions about the Cartesian axes (these errors are often referred to as roll, pitch, and yaw), as shown in Figure 1-1.

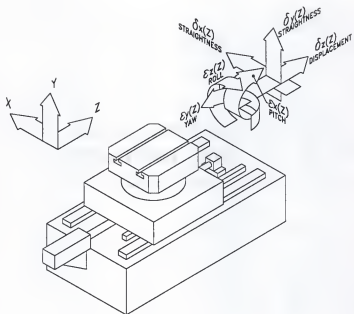


Figure 1-1 Six degrees of error freedom.

Rotary joints also have six degrees of error motion. There is the angular positioning error, an axial error motion, two perpendicular translational motions, and the two remaining angular error motions that are referred to as tilt to distinguish them from the intended angular freedom. These fundamental error motions are often referred to as parametric errors in the literature. Each of these parametric errors propagate through a kinematic chain of joints and bodies, producing a resultant positioning error between the tool and work piece.

Thermal error is the change that occurs in the geometric errors as a result of structural deformation caused by temperature gradients induced from the heat sources. It can be separated into two classifications: drift and kinematic. Drift is the change in position of the tool relative to the work piece at some nominal reference point in the machine and can be seen as the DC offset that occurs in the parametric errors. The kinematic portion is seen as the change in shape of the parametric error motions. Drift can be minimized by the industry accepted practice of periodically probing a reference feature to compensate for the effect in the part program. Minimizing the kinematic changes requires more elaborate techniques, which have not been adopted by industry

Geometric and thermal errors can be mitigated in two ways: error avoidance and error compensation [Blaedel, 1980]. Error avoidance involves eliminating the source of the error, e.g., making perfect machine components, and temperature controlling the machine [Bryan, 1979]. This obviously has physical and fiscal limitations and is not usually a viable solution for commercial machine tools. Error compensation involves canceling the effect of the error by appropriately modifying the machine's commanded

motions. This can be achieved through active compensation or precalibrated compensation. Active compensation involves accurately monitoring the machine's motions against a metrology frame and modifying the commanded motions in real time [Estler and Magrab, 1985]. Precalibrated compensation involves pre-measuring the machine's error motions with reference to some independent variables such as the nominal axes positions and then compensating at a later time based on the errors computed from the independent variables.

Obviously the success of precalibrated compensation depends on and is limited by the machine's repeatability. Precalibrated compensation usually involves making a mathematical model of the machine that is fit to some premeasured data set. The model can be as simple as a look-up table of errors mapped to the machine's scale readings. The errors are predicted based on inputs such as the machine's commanded position and machine temperatures.

Most research has focused on reducing machine tool errors through precalibrated compensation. It has the advantage that it is not prohibitively expensive to install and can be retrofitted to existing machines. Active compensation can be expensive due to the multitude and cost of the dedicated sensors required (laser interferometers). This research focusses on precalibrated compensation, since it has the greatest probability of being adopted by industry.

Precalibrated Compensation

During the past 20 years, the majority of research involving machine tool accuracy enhancement has focussed on precalibrated compensation. Geometric errors are normally addressed by fitting the parametric errors with polynomial equations or placing them in a look-up table for interpolation and then including them in a kinematic model for tool point error prediction. The kinematic model is a mathematical representation used to propagate the parametric errors through the kinematic chain, usually via homogenous transformation matrices. Concatenation of the transformations from one end of the chain to the other results in the positional error of the tool relative to the work table. Correction of geometric errors is only effective at the thermal state in which the errors are measured. Since commercial machine tools do not operate at a single thermal state, geometric compensation alone is not a panacea. Thermal errors must be addressed if significant accuracy enhancement is desired.

Thermal errors are normally addressed by incorporating models that correlate the changing geometric errors to selected temperature inputs around the machine. Models can be as simple as one dimensional parametric fitting of errors to temperature or as complex as the backward propagation neural network [Chen, 1991].

In each of these models, the machine is exercised through a duty cycle with intermittent measurement of the changing geometric errors and temperature sensors. The temperatures and nominal machine positions are used as inputs to the models and the

measured errors are used to determine the terms for the input/output transfer function. After the training set of data is collected, the models predict errors based on nominal machine position and temperature inputs. Temperatures are valid inputs for predicting changing machine geometry because the displacement-strain field in a linear elastic medium is completely defined by the temperature field and the physical boundary conditions.

Previous research involved with thermal error compensation has experienced two major limitations from the available metrology equipment. First, most equipment can not be removed from the work zone during the thermal duty cycle without loss of the measurement reference. Second, most instruments can only measure a single component of error at a time. There have been some recent equipment developments that allow up to five error measurements simultaneously per axis [Ma et al., 1996; Huang and Li, 1996], but these still require multiple set-ups to measure all of the parametric errors.

The first limitation requires a thermal duty cycle free of machining, and the second limitation necessitates a repeat of the cycle for each measurement. This deviates from real machine operation and requires several days of machine down time for measurement. With the introduction of the Laser Ball Bar (LBB), these two limitations can be overcome [Mize, 1993; Ziegert, 1994].

Research Objectives

Geometric and thermal compensation, while proven in the laboratory, has not been implemented on commercial machine tools with the level of proliferation that geometric

compensation has been incorporated on Coordinate Measuring Machines (CMMs). Perhaps geometric compensation has been dismissed because thermal errors can overshadow any improvements. Additionally thermal compensation may appear too complex or appear to be a maintenance nightmare with the multitude of thermal sensors employed. This study attempts to evaluate and compare the amount of benefit obtained from geometric, elementary thermal, and complex thermal compensation models on a 3-1/2 axis machining center. Measurements were made with the Laser Ball Bar (See Appendix 1) developed at the University of Florida and refined by Tetra Precision Incorporated. The geometric model is based on the traditional method of deriving positional error equations using homogeneous transformation matrices. The independent variables for the position error equations are the parametric errors that are measured with the LBB while the machine is in its cold state. The first order thermal model is the geometric model with the addition of linear scale corrections based on scale temperature readings. The complex thermal models comprise a new and unique combination of the deterministic geometric model and a neural network for correlating 31 machine temperatures to changes in the parametric errors. Two neural network models were evaluated. These models are identical with the exception of their training cycles. One of the models was trained with the traditional method of warming the machine by actuation free of machining. The other model was trained by warming the machine with actual machining, since the LBB makes this possible. Comparing these two models will help determine the importance of training with real machining, which until now has been difficult or impossible.

Evaluating accuracy improvement in the context of the complexity of model implementation should provide useful information for a commercial builder in deciding what type of compensation, if any, is most viable for their product.

Tests were conducted on a 3-1/2 axis Cincinnati Milacron Maxim 500 machining center, Figure 1-2. The Maxim has axes travels of 750x700x750 mm (29.5x27.6x29.5 in) in X, Y, and Z respectively. The kinematic structure of the machine has the pallet carried on a moving Z axis carriage running on recirculating linear bearing/ways supported on a cast iron 'T' bed. The spindle is mounted to a Y axis carriage running on recirculating linear bearing/ways on a vertical column. The spindle is rated at 20 KW (33.5 HP) continuous with a maximum speed of 7000 RPM and has 50 V-flange tool holder. The machine is also equipped with a Renishaw MP8 touch trigger probe.

The column runs on X axis recirculating linear bearing/ways mounted to the bed. The pallet is mounted on a B axis indexing table (1/2 axis). A rotating pallet shuttle allows part loading and removal at the front of the machine. A 40 socket tool chain and changer is located opposite the operator station. The controller is a model Acramatic 950 manufactured by Cincinnati Milacron. It has a custom passive backplane computer with multiple i386 based processing boards.

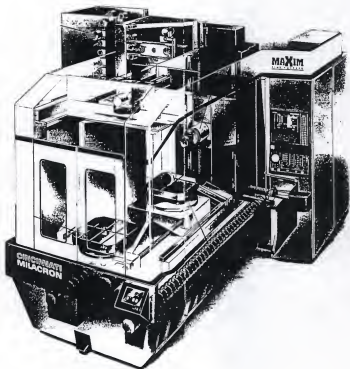


Figure 1-2 Maxim 500 machining center (graphic courtesy of Cincinnati Milacron).

CHAPTER 2 LITERATURE REVIEW

Background

Software compensation of machine tools became possible with the introduction of computer controlled servo systems in the 1950s. Error correction itself predates numerical control [SIP, 1952; Schlesinger, 1927]. The amount of compensation possible was limited to lead screw correction through custom manufactured cams. With the introduction of numerical actuator control, cross compensation of axes became possible. With this advancement, not only could error motions along an axis be corrected, but errors perpendicular to the axis could be corrected through actuation of the other axes as a function of the commanded axis.

Geometric Compensation

Compensating for the errors of the machine at some fixed thermal state, such as the cold state, is often referred to as geometric compensation. Research in this area for CNC machine tools began to take place in the 1960s. Leete first proposed a method to compensate for errors by breaking the feedback loop in the servo system to introduce corrective signals [Leete, 1961]. While he never implemented such a system, several

researchers have since used this technique [Okushima et al., 1975; Donmez 1985, Sumanth 1993].

One of the first documented software corrections of a machine tool was performed by French and Humphries [1967; NIST-60NANB2D1214, 1993]. Backlash and alignment errors were compensated by modifying the part program based on a machine model derived using Euclidian geometry. In the same year, a paper was published detailing the implementation of an online compensation system for a large boring mill [Schede, 1967]. Autocollimators were used for angle measurement and an automatic alignment interferometer provided signals for compensation of machine geometry errors. Similarly, Wong and Koenigsberger also implemented an active compensation system using an optical error detection system [Wong and Koenigsberger, 1967].

Much of the foundation of our modern understanding of measuring and modeling machine tool errors can be attributed to Tlustý [1971]. While no systematic modeling approach was presented, he did mathematically detail the effects each of the angular errors contribute to corresponding linear errors at the tool tip. This is essentially what HTMs accomplish in a more systematic manner. He also introduced a very descriptive nomenclature, that is widely accepted [ASME B5.54], to describe the six degrees of error motion for an axis: $[\delta_x(x), \delta_y(x), \delta_z(x), \epsilon_x(x), \epsilon_y(x), \epsilon_z(x)]$. The Greek delta, δ , represents the translational errors and the subscript denotes the direction of the error. The Greek epsilon, ϵ , represents the angular errors and the subscript denotes the axis about which it rotates. The independent variable inside the parentheses represents the motion axis, x in this example.

One of the first papers dealing with our modern use of software correction was by Wasiukiwicz [1974]. The concept of the machine as an information storage device was introduced. That is, a machine's unique kinematic arrangement and structure serve as an error storage device at least as well as machines repeat their error motions. This is a simple but profound observation. This "memory storage" capability makes precalibrated compensation possible, allowing for instance, cheaper less accurate scales to perform like more accurate and expensive master scales. Wasiukiewicz discusses measuring and storing a three dimensional lattice of errors to be used for correction in the same way scales can be corrected from lookup tables.

The first documented study to incorporate the complete trio of measurement, kinematic modeling, and software correction was presented in a paper by Hocken, et al. at NIST (then NBS) [1977]. The work was performed on a Moore 5-7 coordinate measuring machine. A combination of preprocess gaging and active compensation was utilized as well as intermittent reference probing to mitigate thermal drifts. Parametric measurements were taken over a cubic lattice of two inches and stored in an auxiliary computer for retrieval into a kinematic model made up of 3x3 rotation matrices (a small step away for HTMs). Measuring these errors over a cubic grid allowed non-rigid effects to be included. Schultshik presented a similar paper at the same conference [1977]. Measurements were made on a three-axis jig borer and combined with a rigid body model via matrix mathematics, though not as elegant as Homogeneous Transformation Matrices (HTMs). Unfortunately, he did not use his measurements and model for correction, only verifying the prediction of the model against a ball gage standard, with favorable results.

In the mid 1970s, work continued at NIST on software correction on CMMs and machine tools [NIST-60NANB2D1214, 1993]. Software correction was implemented on a Brown & Sharpe machining center with geometric compensation and temperature correction of the scales (1st order thermal model). Much of this research was applied by commercial CMM manufacturers to correct for geometric errors in their machines.

In 1980 the Machine Tool Task Force at Lawrence Livermore National Laboratory (LLNL) completed its survey of the state of the art [Hocken, 1980; Thusty 1980]. Five volumes were dedicated to accuracy, mechanics, controls, and system management and utilization. A chapter written by Ken Blaedel at LLNL detailed the state of error reduction through avoidance and software compensation. Blaedel makes an interesting analogy regarding predicting a machine's thermal error behavior with that of predicting the weather:

if we had a mathematical model of sufficient sophistication, enough sensors located in the right places, and a large enough high-speed computer to process the data, then one can imagine an NC machine whose control compensates for all thermal deformations. This is a problem of such complexity as to rival that of accurately predicting the weather with the aid of giant computers [Blaedel, 1980, pg. 70]

Thermal Modeling and Compensation

The studies mentioned above demonstrate that software compensation can greatly reduce the effects of geometric error in CMMs and machine tools. Unlike CMMs, geometric error is not the most significant contributor of error for a machine tool. Internal heat sources (e.g. servo motors, guide way friction, cutting energy dissipation), and

changing ambient conditions can cause the geometric errors to change. This problem is not so severe for CMMs which normally have good environmental control and servo systems that operate with very little load. For this reason, machine tool research had to focus on understanding and correcting for thermally induced errors.

A comprehensive survey and in-depth look at thermal errors was conducted by James Bryan [1968]. Bryan surveyed many researchers in the field and presented a heuristic analysis of heat sources, heat transfer mechanisms, and their effects on individual components. He summarized this in a now historic flow chart duplicated in Figure 2-1. He conducted a follow up survey in 1990 to assess the progress since 1967 [Bryan, 1990]. Unfortunately he concluded that little had changed in industry since 1967. However he felt much progress was on the near horizon and that more would be accomplished in the next five years than occurred in the past twenty-three. It appears that this prophesy has yet to be fulfilled.

One of the first documented predictive software thermal models was tested by Ray McClure for his Ph.D. dissertation at Lawrence Livermore laboratories in 1969 [McClure, 1969]. McClure presents an in-depth analysis of thermally induced errors. Error prediction was implemented using lumped parameter models to estimate drift caused by spindle growth on a vertical milling machine. Tests were also conducted to measure the effects of work piece and tool expansion due to the cutting process. Turning tests revealed that using coolant reduced tool expansion by over 80% and reduced part expansion about 60%.

Thermal effects diagram

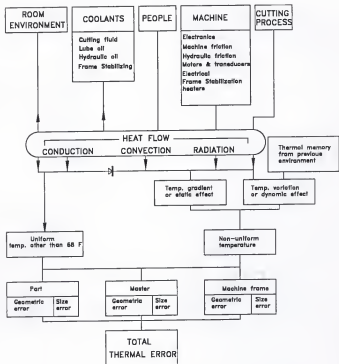


Figure 2-1 Reproduction of heat flow chart [Bryan, 1990].

An important observation was made by Okushima, et al. [1975], that only a few key temperature locations need to be monitored to obtain useful compensation. In this study a vertical machining center was run under no load conditions while temperatures and displacements were measured. Relationships were formulated between temperature and displacement error, and significant error reduction was reported. Thusty and Mutch [1973], also made a similar observation regarding key temperature locations and gave an explanation for their existence. They observed that machine tools typically reach repeatable thermal mode shapes. These mode shapes can be predicted from temperatures at a few key locations.

Many researchers in the early 1980s began to tackle the lowest order thermal effects of drift and scale expansion [Koda and Yoshiro, 1981; Zhang et al., 1985]. Drift is the motion measured between the tool and table at a fixed nominal machine position during changing thermal conditions. It can be caused by thermal growth between the machine's scale reference points, thermally induced bending of machine structure, thermal growth of the end bodies in the kinematic chain, and scale expansion. The predominant solution found in the literature and industry is to probe the tool with a tool setting station or probe a fixed reference artifact to measure the drift [Koda and Yoshiro, 1981, Hocken et al., 1977, Bryan 1990]. Once measured, appropriate compensation moves are undertaken to eliminate the drift.

One of the first complete thermal compensations of a machine tool was performed at NIST by Alkan Donmez on a two-axis turning center [Donmez, 1985]. Parametric errors and selected machine temperatures were measured at discrete intervals as the

machine was warmed up under loadless conditions to steady state and then allowed to cool down to room temperature. The parametric errors were fit with polynomials in both space and temperature. The parametric errors could then be predicted from temperature and nominal machine position inputs. The errors were then input into a kinematic model built using HTMs to compute the tool point error. Correction was achieved by breaking the feedback loop from the rotary encoders and injecting or suppressing pulses. Up to 20 times error reduction was reported.

Donmez's research proved that through a completely deterministic approach, thermal errors could be successfully predicted and compensated. A few commercial applications using thermal modeling began to surface after this research was published [Janeczko, 1988], but only a few rudimentary systems remain commercially available today. Other researchers have followed Donmez's approach of combining polynomial parametric error fitting with HTM modeling [Teeuwsen et al., 1989, Balsamo et al., 1990].

Contemporaneously at Purdue University other researchers were investigating thermal modeling on three-axis machining centers [Venugopal and Barash, 1986]. In this paper, thermoelastic equations were combined with heat transfer equations to show analytically that deformation is instantaneously dependent on the temperature. A finite difference model for temperature prediction was combined with a finite element model to estimate deformations. Like Donmez's work, parametric errors were predicted from a few key temperatures. However, no machining tests were mentioned.

During the early 1990s a new modeling strategy appeared in the literature based

on parallel learning neural networks. In an attempt to extend Donmez's work from a two dimensional to a three dimensional machine, Jenq-Shyong Chen [1991] implemented compensation on a machining center using an artificial neural network model. He used a backward propagating (BP) network which attempts to mimic human synapse/neuron interaction through three layers of nodes with weighted connections between node layers. He also compared the neural network against a multiple regression empirical model by assessing their ability to predict spindle drift. He concluded that the neural network model compared favorably to the multiple regression model. His final test model incorporated both active and predictive compensation. While he concluded that the back propagation ANN was satisfactory, he felt an adaptive resonance theory (ART) network might be more tolerant of noisy input data.

A year later, a BP network was evaluated for use on a two-axis turning center through simulation by Ziegert and Kalle [1994]. They assumed realistic functions for the parametric errors and computed volumetric errors with a kinematic model to train the network. The simulation indicated accurate prediction of error might be possible and this was verified experimentally by Srinivasa, Ziegert, and Smith on a two-axis turning center [1993]. Like Chen, Srinivasa noted drawbacks to the BP network which included, long training times, trial and error selection of the network architecture, and a vagueness of how the network parameters relate to real world parameters. Because of these shortcomings, Srinivasa adapted a fuzzy ART map network to predict the compensation values for the same two-axis turning center used in his previous work at the University of Florida [Srinivasa, 1994]. Srinivasa trained the ART map by intermittently measuring

volumetric errors with the LBB as the machine was warmed through non-machining actuation and allowed to cool. Only a single thermal cycle was needed because all the necessary errors for training could be collected simultaneously with the LBB. Cutting tests revealed that the ART map correction system improved feature accuracies by 2.0 to 15.3 times.

A interesting use of thermal imaging was used to investigate the temperature gradients of a machine tool during a thermal duty cycle [Allen et al., 1996]. Thermal imaging revealed unexpected heat sources on a three-axis machining center. The imaging was also used to locate key locations that were subsequently monitored to predict thermal drift. A reduction in drift from $70\mu\text{m}$ to $10\mu\text{m}$ over a three hour duty cycle was achieved.

A recent study at the Department of Precision Instrument Engineering, Tianjin University China, modeled the effects of thermal errors by correlating them to spindle speed as opposed to temperatures [Shuhe et al., 1997]. Measurements were made with a 1-D ball array for errors in the Z direction. The errors were correlated to the spindle speed at four locations on the Z axis using least squares fit. The errors were compensated by premodifying the part program based on its spindle speed requirements. A simple 1-D depth cutting test was performed with and without compensation after 1 hour of operation. An error reduction from $7\mu\text{m}$ to $2\mu\text{m}$ was reported.

While no thermal modeling was conducted, it is appropriate to mention recent research that occurred at Lawrence Livermore National Labs [Krulwich et al., 1995]. Krulwich utilized the LBB for measurement and error compensation on the same

Cincinnati Milacron Maxim 500 used in this research. Krulewich introduced a new measurement technique she termed the projection method. It consists of measuring lengths between two magnetic sockets and projecting the length along the nominal direction between the two sockets. The nominal direction, or vector, is obtained from knowledge of the approximate location of the sockets in the machine's coordinate frame. The error of the projected length is used to fit the parameters of a rigid body kinematic model with assumed polynomial fits to the parametric errors. The projection method allows for an extended work volume over trilateration with the LBB since for a given position the length measurement between each base socket is not required. The method relies on the assumption of knowing the nominal position of the sockets to within about 1.5 mm (0.062 in).

Three thousand lengths were taken over a 3 ½ hour period to fit the model with linear regression techniques. The model was tested by measuring face and body diagonals with a laser interferometer. The predicted errors were within about $\pm 2.0 \mu\text{m}$ for approximate 800mm diagonals. Compensation was also carried out using part program modification with nearly equal results.

Motivation for the Research

Based on the above literature survey it is evident that significant geometric and thermal error reduction is possible. CMM manufacturers have realized this and incorporated geometric compensation in almost every machine sold today. Machine tool builders have not followed their lead. While dramatic improvements have been

demonstrated for at least the last 15 years, most machine tools sold today have only geometric scale compensation systems incorporated. Perhaps builders have not taken the next step of full geometric compensation because the thermal errors appear so overwhelming. As mentioned earlier, thermal errors are not an issue for CMMs. It is understandable that the thermal compensation schemes demonstrated by researchers might make a builder reluctant to implement such systems. The many temperature sensors normally used would surely increase the maintenance level on a machine. The perceived benefits apparently do not outweigh the perceived complexity in the machine tool builder's and user's minds.

Scope of the Research

In an attempt to assess the benefit/complexity trade off, the performance enhancement of three thermal compensation models was evaluated against geometric compensation and no compensation on a three-axis machining center. The geometric compensation model is included to further reference how much thermal effects contribute to the overall error.

The first thermal model evaluated was the simple first order scale compensation model utilized by earlier researchers[NIST-60NANB2D1214, 1993; Koda and Yoshiro, 1981; Zhang et al., 1985]. It is based on elementary physics and requires only four thermal sensors. Nowhere in the literature search has a comparison been made to see how much is really gained over this simple completely deterministic model.

The remaining two thermal models utilize the fuzzy ART map refined by Srinivasa

in a new implementation that combines it with kinematic modeling. One network was trained using a traditional no load actuation thermal duty cycle and the other was trained with a machining thermal duty cycle. This serves to quantify what errors are being missed when the machine is measured by the common practice of excluding actual machining.

These models were evaluated at different thermal states by measuring body diagonals with the Laser Ball Bar and by machining the B5.54 precision positioning test part [ASME B5.54, 1992]. Thermal drift was addressed by using the industry accepted practice of probing a reference feature.

All of the models utilized rigid body kinematics via homogeneous transformation matrices. This type of model has proven successful in the research, but no testing of its durability was found. Machine tool users will want to minimize the frequency of the measurements for their models as much as possible. To address this, a durability test will be conducted over several months to see how a model degrades.

From the tests mentioned above, the data was examined to shed light on the five following areas: 1. success of implementing the Fuzzy ART-MAP to a 3D milling machine, 2. model durability, 3. geometric modeling vs. thermal modeling, 4. deterministic vs. non-deterministic modeling, 5. training with machining and without.

Chapter 3 describes the geometric model that was used and incorporated into the thermal models. Chapter 4 describes the three thermal models employed. Chapter 5 details the measurement and machining procedures. Chapter 6 presents the results of the durability tests, body diagonal measurements, and machined part tests. Chapter 7 draws appropriate conclusions and makes suggestions for future work in this area.

CHAPTER 3 GEOMETRIC MODEL

Geometric Compensation

A machine tool's thermal error can be considered as geometric error with an additional dependence on the machine's thermal state. In this definition, geometric error is the machine's error at some given thermal state, usually the power on, machine idle, steady state. Each thermal model evaluated in this study is built from the same geometric model. The models only differ in how the variables to the geometric model are modified with respect to temperature. The geometric model is a function of the machine's parametric error motions:

$$GEOMETRIC = F\{\delta_i(X), \delta_i(Y), \delta_i(Z), \varepsilon_i(X), \varepsilon_i(Y), \varepsilon_i(Z)\}$$

i - index representing the X, Y, and Z axes

and the machine's parametric errors gain a dependence on the thermal state in the thermal model:

$$\gamma_{THERMAL} = F\{\delta_i(X, T), \delta_i(Y, T), \delta_i(Z, T), \varepsilon_i(X, T), \varepsilon_i(Y, T), \varepsilon_i(Z, T)\}$$

T - temperature field of the machine.

The geometric model utilized is the successfully demonstrated kinematic joint chain model mathematically represented with homogeneous transformation matrices [Donmez, 1985; Chen, 1991; Mize, 1993] and will hence be referred to as the Homogenous Transformation Matrix model, HTM model.

In an HTM model, the machine is represented as an open loop chain of rigid bodies connected by rotary or prismatic joints. The chain is open between the work table and the tool. The work piece fills this opening and closes the chain. HTMs mathematically relate the position and orientation of one body relative to the next body in the kinematic chain and can be used to transform vectors between coordinate systems. This matrix representation was introduced by Denavit and Hartenberg [1955], as a systematic method to compute the position of a robot end effector based on its joint positions.

In the notation representing the transformation, T_j^I , the superscript, I , denotes the reference frame and the subscript, j , denotes the current frame. Premultiplying a vector described in the current frame by this transformation matrix will produce the vector described in the base frame. The 3x3 matrix bounded by the first three rows and the first three columns contains the orientation information between frames and is called the rotation matrix. The columns of this 3x3 matrix are the unit vectors of the current frame's axes as described in the reference frame. The first three terms of the last column are the components of the position vector from the origin of the reference frame to the origin of the current frame, as described in the base reference. The last row is set to (0 0 0 1) for our purposes. Other choices for the last row result in non-homogeneous transformations which do not, in general, preserve lengths and angles. A convenient feature of HTMs is

that they can be multiplied in series to obtain a resultant HTM between two frames (e.g. ${}^0T_2 = {}^0T_1 {}^1T_2$).

A fundamental assumption implied in the model is that the bodies are rigid, i.e., that deflections of the bodies due to gravity and loading are negligible. This assumption generally holds true in machine tools since positioning accuracy and good cutting dynamics require very stiff machine components. However, if non-rigid effects are significant, their effects will only be modeled if they are present at the machine positions selected for parametric error measurements.

The HTM model requires measurements of all six degrees of error motion for each moving body in the kinematic chain. For a 3 axis machine this results in 18 error measurements. Traditionally the three orthogonalities between the axes are also included in the total, resulting in 21 errors. However for modeling, it is convenient to include the squareness errors into the appropriate straightness errors since squareness is merely straightness with a linear dependence on position. When straightness has squareness included it has been appropriately referred to as lateral error to distinguish between the two [Tlusty, 1980].

Kinematic Model for the Machining Center

The construction of the model begins by assigning coordinate systems to each body in the kinematic chain. For the 3-½ axis machine, ignoring the 'B' axis, we begin by placing a coordinate system on the work table. This will be the frame of reference, since this is the frame where the work piece is machined, see Figure 3-1. Working through the

chain, a frame is attached to the bed of the machine, then the 'X' carriage, and finally to the tool itself. It is important to note that frame placement is arbitrary. A frame does not even have to be within the physical bounds of the body. A frame can be placed outside the bounds of the body and an assumed imaginary rigid attachment back to the body. The goal of the HTM model is to know the error of the tool in the reference frame. For error-free motion and assuming that all of the frames are coincident at some initial start position, the three transformation matrices between the bodies on the machine are as follows:

$${}^0T_1 = \begin{bmatrix} 1 & 0 & 0 & 0 \\ 0 & 1 & 0 & 0 \\ 0 & 0 & 1 & Z \\ 0 & 0 & 0 & 1 \end{bmatrix} \quad {}^1T_2 = \begin{bmatrix} 1 & 0 & 0 & X \\ 0 & 1 & 0 & 0 \\ 0 & 0 & 1 & 0 \\ 0 & 0 & 0 & 1 \end{bmatrix} \quad {}^2T_3 = \begin{bmatrix} 1 & 0 & 0 & 0 \\ 0 & 1 & 0 & Y \\ 0 & 0 & 1 & 0 \\ 0 & 0 & 0 & 1 \end{bmatrix}$$

Since each body's motion is not free of error, the error motions need to be included. These are easily included by including an additional transformation for each body's perfect motion that is due to the error motion. The true transformations between bodies then becomes $[T] = [T][E]$, where

$$E = \begin{bmatrix} 1 & -e_x(i) & e_y(i) & \delta_x(i) \\ e_x(i) & 1 & -e_y(i) & \delta_y(i) \\ -e_y(i) & e_x(i) & 1 & \delta_z(i) \\ 0 & 0 & 0 & 1 \end{bmatrix}$$

i - index representing the prismatic axes

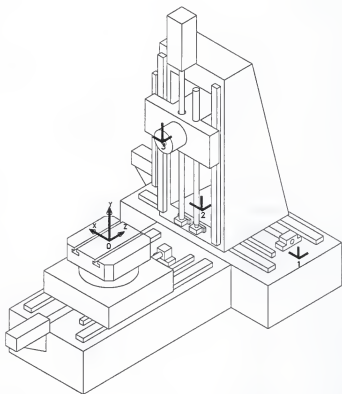


Figure 3-1 Machine coordinate frame assignment.

The error matrix is valid for small error motions where higher order terms can be ignored.

The actual transformations then become

$${}^0T_1 = \begin{bmatrix} 1 & -\varepsilon_z(Z) & \varepsilon_y(Z) & \delta_x(Z) \\ \varepsilon_x(Z) & 1 & -\varepsilon_x(Z) & \delta_y(Z) \\ -\varepsilon_y(Z) & \varepsilon_x(Z) & 1 & Z + \delta_z(Z) \\ 0 & 0 & 0 & 1 \end{bmatrix}$$

$${}^1T_2 = \begin{bmatrix} 1 & -\varepsilon_z(X) & \varepsilon_y(X) & \delta_x(X) + X \\ \varepsilon_x(X) & 1 & -\varepsilon_x(X) & \delta_y(X) \\ -\varepsilon_y(X) & \varepsilon_x(X) & 1 & \delta_z(X) \\ 0 & 0 & 0 & 1 \end{bmatrix}$$

$${}^2T_3 = \begin{bmatrix} 1 & -\varepsilon_z(Y) & \varepsilon_y(Y) & \delta_x(Y) \\ \varepsilon_x(Y) & 1 & -\varepsilon_x(Y) & \delta_y + Y \\ -\varepsilon_y(Y) & \varepsilon_x(Y) & 1 & \delta_z(Y) \\ 0 & 0 & 0 & 1 \end{bmatrix}$$

Concatenating the matrices from the work table frame to the tool frame, ${}^0T_3 = {}^0T_1$
 ${}^1T_2 {}^2T_3$, a transformation is obtained that transforms a vector in the tool frame into the
 work table frame. For a given point in the tool frame, premultiplying it by the 0T_3 frame
 will describe the point in the work table frame. Realizing that any point described in the
 tool system not its origin is a tool offset, we can determine the actual position of the tool

for a given offset as

$$\begin{Bmatrix} X_A \\ Y_A \\ Z_A \end{Bmatrix}_{ACTUAL} = {}^0T_3 \begin{Bmatrix} X_T \\ Y_T \\ Z_T \end{Bmatrix}_{TOOL}$$

With the actual position determined, the error can be computed as:

$$ERROR = \vec{X}_A - \vec{X}_C ; \vec{X}_C = \vec{X}_{NOMINAL} + \vec{X}_T$$

X_A - Actual position

X_C - Commanded position

$X_{NOMINAL}$ - Commanded position of gage point

X_T - Tool offset from gage point

Carrying out the matrix manipulations, neglecting higher order terms, and substituting into the above equation, the error equations are obtained:

$$P_X = \delta_X(X) + \delta_X(Y) + \delta_X(Z) - Y\{e_Z(X) + e_Z(Z)\} - Y_T\{e_Z(X) + e_Z(Y) + e_Z(Z)\} \\ + Z_T\{e_Y(X) + e_Y(Y) + e_Y(Z)\}$$

$$P_Y = \delta_Y(X) + \delta_Y(Y) + \delta_Y(Z) + Xe_Z(Z) + X_T\{e_Z(X) + e_Z(Z)\} \\ - Z_T\{e_X(X) + e_X(Y) + e_X(Z)\}$$

$$P_Z = \delta_Z(X) + \delta_Z(Y) + \delta_Z(Z) - Xe_Y(Z) - X_T\{e_Y(X) + e_Y(Y) + e_Y(Z)\} \\ + Y\{e_X(X) + e_X(Z)\} + Y_T\{e_X(X) + e_X(Y) + e_X(Z)\}$$

The values X, Y and Z in the equations are the nominal machine coordinates from the machine point where all of the errors are initially assumed to be zero. In this

application, this occurs at the intersection of the three measurement lines (0, 280, 340)mm. This is the basic geometric model. Thermal effects are included by modeling each parametric error with temperature as well as position, e.g., $\delta x(X, T_0, T_1, \dots, T_n)$.

Implementation in the Controller

The geometric model is implemented inside the A950 controller. Each of the 18 parametric errors are least squares fit with 4th order polynomials with respect to axis position. Reversal errors for each of the 18 parametric errors are stored as a single coefficient computed as the average reversal error from the measurements. Squareness has been included in the appropriate straightness coefficients, 1st order terms of straightness errors. The coefficients for the polynomials are stored in a table that can be updated through the parallel port on the controller. The polynomials and three error equations shown above, are executed in a peripheral board running inside the control computer autonomous from the servo control loop, and the program is shown in Appendix B. This i386 based board monitors the axes positions and computes the positioning error to modify the nominal position at every closure of the feedback loop (approximately 5 ms). A block diagram of the servo system with the compensation is shown in Figure 3-2. The thermal modeling was implemented by changing the appropriate coefficients in the table based on temperatures monitored around the machine, and is discussed in the next chapter.

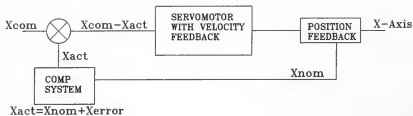


Figure 3-2 Block diagram of compensation system.

CHAPTER 4 THERMAL ERROR MODELS

Introduction

As mentioned previously, thermally induced error was compensated by modifying the parametric error inputs in the kinematic model as a function of temperature as opposed to directly correlating temperature to the volumetric errors. This is a valid deterministic approach, since the parametric errors are known to change with temperature and the volumetric errors can be predicted via the parametric errors and a kinematic model. Three thermal models were evaluated that follow this general approach. Only the method by which the parametric errors are correlated to temperature will differ.

The simplest model to be evaluated deals with only the linear variation of the displacement errors with temperature. It is based on the elementary physics of material expansion and contraction. The remaining two models utilize the fuzzy ART network developed by Srinivasa in a new implementation to predict all 18 of the parametric errors based on temperature inputs from the machine [Srinivasa, 1994]. These two models differ only in their training cycle. One is trained with the traditional method of machine warm up using axis and spindle actuation free of machining. The other uses actual machining

in its warm up cycle to more closely model realistic use.

First Order Thermal Model

The first level of thermal compensation is naturally to compensate for the thermal expansion and contraction of the scales. This error results in a one to one error at the tool, e.g., an 'X' scale error of 1 μm will contribute 1 μm of tool 'X' coordinate error. The scale error can be represented by the formula

$$\delta_X(X, T_{\text{scale}}) = \delta_X(X)_{\text{REF}} + \int \alpha(T(X)) [T(X)_{\text{scale}} - T_{\text{REF}}] dX$$

$\delta_X(X)_{\text{REF}}$ - Scale error at some reference temperature
 $\alpha(T(X))$ - Temperature dependent coefficient of expansion
 T_{REF} - Reference temperature scale is measured at

Assuming a uniform temperature distribution and a constant coefficient of expansion, the equation reduces to

$$\delta_X(X, T_{\text{scale}}) = \delta_X(X) + \alpha [T_{\text{scale}} - T_{\text{REF}}] X$$

The thermal portion of this error manifests itself in lead screw expansion for rotary encoder feed back systems, and in scale expansion for glass scales and other solid linear metrics. Laser interferometer scales have a similar error based on atmospheric wavelength variation with temperature, although the dependency is typically an order of magnitude less.

This model has been chosen for comparison, because it is thought to be the most readily accepted by industry. It is understandable that industry might shy away from more complex models that require many thermal sensors (>10) and their associated

maintenance. This model utilizes 4 sensors, one for each axis and one for the work piece. The literature review did not reveal any comparisons between more elaborate thermal models and this simple model based on elementary physics.

Implementation of the Model

A temperature sensor, in this case a "T" type thermocouple, has been placed on the metallic housing surrounding each glass scale at its mid-span. The effectiveness of this placement depends on the homogeneity of the scale temperature and the similarity of the housing temperature to the actual scale temperature. The scales on the Maxim are contained in an aluminum housing anchored at their midpoint to the machine structure. Heat transfer is primarily from natural convection, so the homogeneity assumption should be reasonable. The 'Y' axis scale is most likely to deviate from this assumption since it has a vertical orientation that is more susceptible to vertical temperature gradients. Multiple sensors could be placed along the length of the scale and included in a piecewise integration to handle the gradients, but this digresses from the simple model objective of as few sensors as possible. A sensor is also placed on the work piece to get an estimate of the part's bulk temperature. This is used to compensate the scale to expand and contract like the work piece material at its bulk temperature. This should help to minimize errors caused by differing material/scale expansions when either the scale's or part's temperature deviates from the international temperature standard of 20°C. Thermal gradients will surely exist in the part as a result of local heat transfer from the cutting process, however coolant fluid will be used to minimize the effect. The system as stated,

is only capable of compensating for that portion of the part thermal expansion that is equivalent to the temperature as read by the work piece sensor.

The data collection procedure requires the scale temperature, T_{ref} , be recorded as the displacement errors are measured. The displacement correction can then be modified to make the scale expand and contract like the part material.

The error of the scale to be corrected is

$$SCALE\ ERROR = \delta_x(X) + [(T_{scale} - T_{REF})\alpha_{scale} - (T_{part} - 20^{\circ}C)\alpha_{part}]X$$

By correcting the scale's displacement error, $\delta_x(X)$, at a reference temperature, T_{REF} , the temperature sensor's absolute temperature accuracy is not important, only its relative accuracy. Thermocouples are well suited for relative accuracy over limited temperature ranges. However, the material correction to $20^{\circ}C$ does require accurate absolute temperature measurement, and for this reason a thermistor is used. The term $[(T_{scale} - T_{ref})\alpha_{scale} - (T_{part} - 20^{\circ}C)\alpha_{part}]$ is added to the 1st order coefficient in the 4th order curve fit of the displacement errors.

Thermal Drift

This model does not have the capability to compensate for all sources of thermal drift. Drift can be caused by thermal expansion/contraction of the material between the scale anchor points. It can be caused by thermal expansion/contraction of the material between the scale read head and the tool or work piece. Thermal drift can also be caused by the scale expansion/contraction, which is the only source this model is capable of addressing. Instead drift will be addressed by the industry accepted practice of probing

a reference feature on the part or machine prior to machining which mitigates all drift sources.

The Neural Network Model

Because the relationship between machine tool error and the thermal state of the machine is complex and beyond all but the most complex deterministic approaches, Artificial Neural Networks (ANN) have been employed to mimic the thermal/error relationship [Chen, 1991; Ziegert and Kalle, 1994; Srinivasa, 1994]. The network mimics the relationship, because ANN's do not express this relationship based on the physics of heat transfer and solid mechanics like finite element modeling. Rather, they develop a relationship between empirically generated inputs and outputs based on a set of rules. The ANN evaluated in this study is based on the ART MAP developed by Carpenter et al. [1991], and refined for machine tools by Srinivasa [1994].

In simplest terms, the ART MAP categorizes a set of input vectors into discrete classes and maps these input classes to corresponding categorized output vector classes. In our case, the components of the input vectors are composed of the temperature sensor readouts, the output vectors are the coefficients of the polynomial fits to the parametric errors. Neural networks have two operating modes, training, and prediction. Neural networks must first be trained on empirical data before prediction can take place.

During training, a new input vector is introduced and is compared to the existing classes to see if a match exists or if the vector is a new unique class. A class is defined as a unique input vector, where uniqueness is judged by a fuzzy logic comparison to the

existing classes. This comparison is made via a fuzzy logic equation whose output is a similarity factor called vigilance, represented by the Greek letter rho.

$$\rho_J \leq \frac{|X \wedge W_J|}{|X^A|} = \frac{\sum \min(X_i, W_{Ji})}{\sum X_i}$$

\wedge - fuzzy AND operator.

i - index for the vector component.

J - index for the existing classe being compared.

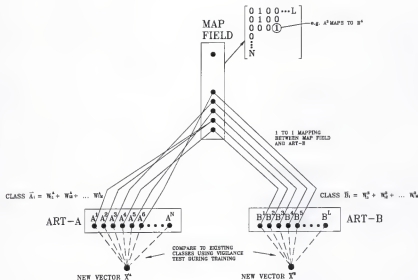
X - vector to be compared.

W - class vector.

Vigilance can range between zero and one. A vigilance of one is achieved if a vector matches a class exactly. If the vigilance between a vector and an existing class is larger than a user defined threshold, it is considered to be equivalent to the class. If the input vector fails to meet this threshold similarity with any of the existing classes, it is considered to be a new and unique class.

Simultaneously the same procedure is performed on the output vectors. Additional logic insures that the input classes map to only one output class. However, an output class can be mapped from more than one input class. If an output vector is found to be unique, but its corresponding input is not, the input is forced, by changing the vigilance threshold, to become a unique class. Figure 4-1, shows a graphical representation of the network.

The fuzzy ART-MAP can be thought of as an algorithm that identifies similarity in input and output data sets to minimize redundancy, and maps the remaining input data to the remaining output data sets. After training, the network is used to predict machine



RULES:

TRAINING:

1. NEW INPUT AND OUTPUT VECTORS ARE COMPARED TO EXISTING CLASSES FOR UNIQUENESS USING VIGILANCE TEST.
2. IF FOUND TO BE UNIQUE, NEW CLASS IS FORMED.
3. IF NEW OUTPUT CLASS IS FORMED AND NOT A NEW INPUT CLASS, INPUT VIGILANCE IS RESET TO FORCE INPUT TO BE A NEW CLASS.
4. IF EITHER INPUT OR OUTPUT IS FOUND TO MATCH AN EXISTING CLASS, WEIGHTS TO THE CLASS ARE MODIFIED APPROPRIATELY.

PREDICTION:

1. INPUT VECTOR IS COMPARED TO EXISTING CLASSES IN ART-A USING ACTIVITY PATTERN, AND CLASS WITH HIGHEST ACTIVITY IS CHOSEN.
2. SELECTED CLASS "A" IS INPUT INTO MAP FIELD TO FIND CORRESPONDING OUTPUT MATCH.

Figure 4-1 Schematic representation of fuzzy ART-MAP.

tool parametric errors by comparing new input vectors to the existing classes using another fuzzy logic comparison. The fuzzy logic equation for comparison is called the activity pattern:

$$T_J(X^A) = \frac{|X^A \wedge W_J^A|}{|W_J^A|} = \frac{\sum \min(X_i, W_{ji})}{\sum W_j^A}$$

- \wedge - fuzzy AND operator.
- i - index for the vector component.
- J - index representing class number.
- X - Input vector to be compared.
- W - Existing class to be compared

The class that exhibits the most similarity based on this fuzzy logic test, is selected and its corresponding output vector is the predicted error. The FAM's ability to predict accurately is limited by the similarity of the training set to that of inputs presented to it. Therefore, it is critical to present diverse inputs during training, to assure all real-world thermal states are included.

Incorporation of the Network in the Model

The neural network can be utilized for mapping a variety of input/output feature sets. The selection of where a network or networks is included in the model will be an important factor in the model's performance. For instance, a network could be the model itself if it were used to predict all three components of the volumetric error based on inputs of temperature and position. This is similar to the approach Srinivasa used for compensating the two dimensional errors of a lathe [Srinivasa, 1994]. However, such an

approach discards any deterministic solutions to the problem.

At the other end of the spectrum, networks could be used to predict each of the parametric errors for input into a rigid body kinematic model. This would retain the proven deterministic technique of computing volumetric error from the parametric errors, and dedicate the network to mimicking the complex relationship of the parametric errors with temperature and position. This architecture was considered for our model, but was excluded for fear of attenuation of the positional inputs due to the more numerous temperature inputs. Because all inputs in an ART-MAP inherently have equal weight, the large number of temperatures, 31, could overshadow the 3 positional inputs. Srinivasa experienced a similar problem with directional inputs in his model [1994]. He used an ART-MAP to predict a single component of the 2D error vector on a lathe from the 2D position input and selected temperatures. Originally his networks had an input for axis direction. He found that the networks could not successfully predict errors of reversal with this architecture and he opted to use separate networks for axis direction.

With this in mind, the approach is to avoid overworking the network and allow it to handle only that part of the problem for which the deterministic approach has failed or been overly complex to implement. Considering that the deformation field of an elastic medium is uniquely determined from its temperature field and its kinematic boundary conditions, a machine's deformations might be reasonably dependent on its temperature field since the kinematic boundary conditions are relatively fixed. Realizing that the variation of the parametric errors can be attributed to changes in the machine's geometry, networks will be used to predict the parametric errors from selected temperature inputs.

Axes position will be eliminated as a direct input by using the network to predict the coefficients of a 4th order least squares polynomial. The coefficients to the polynomial inherently describe the error with respect to position, eliminating it as a direct input.

At each measurement cycle, the parametric errors are fit to 4th order polynomial equations. The average reversal error for each parametric error is also computed and included as an extra coefficient.

The coefficients are predicted from the temperatures using seven networks. The input/output relationship of each network is shown in Table 4-1. Each of the scale error coefficients are predicted from a single network using the scale's temperature sensor as an input. This retains the deterministic part of the solution in which thermal scale error is known to be purely a function of its temperature distribution. The remaining parametric error coefficients are mapped to the temperature sensors on the body supporting their prismatic axis. For example, the X-Axis angular and straightness parametric error coefficients are mapped to the temperature sensors on the bed where the X-Axis ways are mounted. This assumes that these errors are a function of their way's shape. Finally a single network is used to map the parametric error drifts to all 31 temperature sensors, since the deformation of each body in the kinematic chain can contribute to drift.

This type of architecture was selected to retain the proven deterministic technique of computing volumetric errors from the parametric errors, minimizing the task of the networks to determining the thermal dependence of the parametric errors. This is thought to be a good application for an ART-MAP network, since they are good at selecting the closest match to a finite number of selections. When measured parametric errors are

TABLE 4-1

NETWORK INPUT/OUTPUT RELATIONSHIP		
NETWORK	TEMP INPUTS*	COEFF OUTPUTS
1	T25	X DISPLACEMENT
2	T11	Y DISPLACEMENT
3	T2	Z DISPLACEMENT
4	T21,T23,T28,T30	X ANGULAR AND STRAIGHTNESS
5	T1,T4,T5,T8,T9,T13,T14,T17,T20,T24,T26,T27	Y ANGULAR AND STRAIGHTNESS
6	T3,T6,T7,T10	Z ANGULAR AND STRAIGHTNESS
7	T1-T31	PARAMETRIC ERROR DRIFTS

* See Figure 4-4 for temperature sensor location

plotted with their drift removed, curves tend to maintain their form and at most change slope, Figure 4-2. Therefore, over a thermal duty cycle, selecting a curve from the finite choices, is unlikely to be in great error since adjacent curves do not differ greatly.

Implementation on the Machine

In this study, two different training sets are evaluated: 1. warm-up without machining, and 2. warm-up with machining. The literature review revealed no instance where actual machining was utilized in the training cycle. The reason probably involves the delicacy and incremental nature of the measurement transducers. Most measurement transducers can only measure changes in their measurement parameter, not absolute values. Laser interferometers, one of the more common metrology instruments, can only measure changes in length (displacement), and can therefore not measure thermal drift if

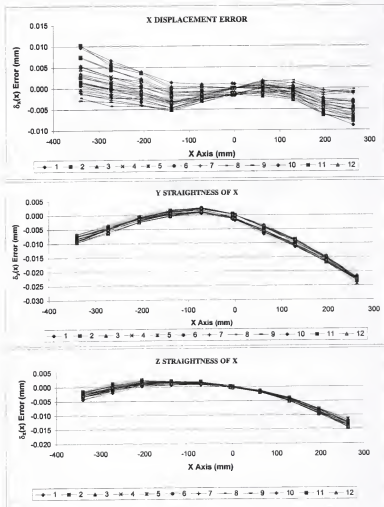


Figure 4-2 Typical parametric errors at different thermal states.

their signal is interrupted by machining operations. Also their operation is restricted to linear motion, further neglecting any useful machining.

The LBB overcomes the incremental measurement problem because it is initialized to an absolute distance and trilateration produces absolute coordinates. It can therefore be removed from the work zone during machining and reintroduced after, without loss of reference. No loss of reference occurs as long as the magnetic sockets are not disturbed from their original placement. They can move due to thermal contraction and expansion of the machine elements, but this is merely the thermal drifting of the machine we intend to measure. Also, any change in distance between the base sockets will be accounted for by their measurement before each cycle. We are able to machine parts without disturbing the socket placements, because the sockets on the spindle are mounted on the periphery of the spindle housing allowing the simultaneous use of a cutting tool, Figure 4-3. Also the pallet with the base sockets can be shuttled out while a part is shuttled in for machining. By shuttling the pallet with the sockets in and out, we are depending on the repeatability of the pallet relocation with respect to the Z axis carriage. Repeatability tests were conducted by shuttling the pallet in and out several times and measuring the location of a socket mounted on the spindle each time. The results are shown in Table 4-2. This repeatability will limit the accuracy of the translational drift measurement.

TABLE 4-2

Pallet Change Repeatability (Max variation of 10 runs)		
X Axis	Y Axis	Z Axis
3.3 μ m	4.0 μ m	1.6 μ m

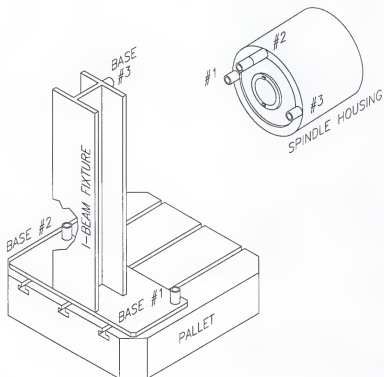


Figure 4-3 Socket placement on the machine.

A small compromise was also utilized in placing the sockets on the periphery of the spindle. This was done because fixturing the sockets on a tool holder was found to be too compliant. When the LBB is in a socket that is offset from the spindle center line, enough torque is produced to cause unwanted rotation of the spindle. The servo locking mechanism also tends to hunt. By not fixturing to the spindle, a small part of the kinematic chain is bypassed. Any growth or drifting of the rotating portion of the spindle relative to the housing will be missed. However, the socket placement on the housing is very near the bearing connection to the spindle and any lost drift motion is thought to be outweighed by the gain in socket rigidity.

The non-machining duty cycle is similar to that implemented by other researchers [Donmez, 1985; Chen, 1991; Srinivasa, 1994]. It involves actuating the axes and spindle at predetermined speeds and feeds, followed by an idle "machine on" cool down period with intermittent pauses taken for measurement. Two thermal cycles were utilized over two days for training. The first thermal cycle consisted of the spindle operating at 2500 RPM and the three axes actuated at 5 m/min for 30 minutes, followed by a measurement. This routine was repeated continuously over an eight hour period. After this warm-up period, the machine was left in the idle power on state for four hours. Measurements were taken after 30 minutes and then every hour after that. The second thermal cycle was identical except that the spindle was operated at 5000 RPM and the axes were operated at 10 m/min.

For the machining duty cycle, a production machine run was emulated, in which an identical part or part features is/are repeatedly machined over a single shift day.

During this shift, several parts will typically be loaded, machined, and removed. This cycle was emulated by machining for 30 minutes, cooling down for 10 minutes, and measuring for 20 minutes. The machining consisted of a facing operation with an insert type face mill in 6061 aluminum. Training occurred over two days so that different metal removal rates could be used for the warm-up cycle. The first training cycle used a metal removal rate of $76,200 \text{ mm}^3/\text{min}$, for an approximate power consumption from the spindle of 1 kW. The second training cycle used a metal removal rate of $381,000 \text{ mm}^3/\text{min}$, for an approximate power consumption from the spindle of 5 kW. These 60 minute cycles were repeated over an 8 hour period. The cool down portion of the duty cycle was the same as for the non-machining duty cycle, idle machine state for 4 hours, with measurement after the first half hour followed by measurements approximately every hour.

Thermal Sensor Placement

The prediction capability of the neural network is dependent on the placement of the thermal sensors on the machine. For this study, 'T' type thermocouples were utilized as the temperature sensors. They were interfaced to a i486-33Mhz computer through a National Instruments multiplexer board with cold junction compensation and a 16 bit analog to digital converter with programmable gains. The multiplexer allows 31 thermocouples to be used. Each thermocouple input into the analog to digital converter was conditioned with a low pass filter providing a cutoff frequency of 4 Hz with -3 db attenuation and then amplified with a gain of 100. The filtering was necessary to reduce noise pick up from the servo motors and transformers. This system provides 0.04°C of

resolution, but noise limits the useful resolution to about 0.1°C . Placement of the thermocouples is shown in Figure 4-4.

Locations were selected based on engineering judgement. Preference was given to the Y column due to its proximity to the primary heat source, spindle motor, and its relatively small mass. Sensors were placed along the front and back of the Y column on both sides to allow the network to recognize any significant gradients that might cause bending. Similarly, the spindle housing was instrumented around its relatively unconstrained periphery. Both the X and Z beds were instrumented along their top surfaces. Deformation of their bottom surfaces is constrained by 13 mounting pads epoxied to a 12" thick concrete floor. Each glass scale was also instrumented with a thermocouple on its housing at mid-span.

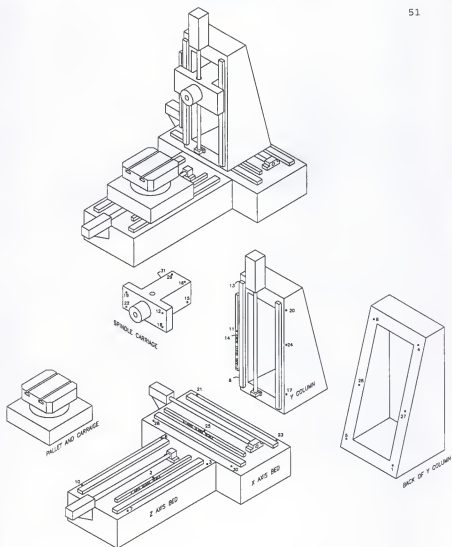


Figure 4-4 Thermal sensor placement on the machine.

CHAPTER 5 MEASUREMENT AND MACHINING PROCEDURES

Geometric Error Measurement with the Laser Ball Bar

Because evaluation of thermal error is accomplished by measuring the machine's geometric error at different thermal states, there are only parametric error measurement techniques to be discussed. As was mentioned in Chapter 3, the geometric (or volumetric) errors for a machine can be reliably represented by the machine's parametric errors and a rigid body kinematic model, the HTM model. Utilizing the LBB's volumetric measurement capability, the parametric errors can be decomposed from a series of volumetric measurements.

Trilateration of a single point on a body as it moves along an axis, 'T', directly provides the translational parametric errors $[\delta x(I), \delta y(I), \delta z(I)]$ for that body. To measure angular parametric errors $[\epsilon x(I), \epsilon y(I), \epsilon z(I)]$ with the LBB, the volumetric position of at least three points on the moving body must be known; three non-collinear points on a rigid body uniquely define its orientation and position. This can be accomplished by trilaterating to three points on the moving body. This requires measuring nine variable

leg lengths. However, this actually provides redundant information. Only six distances between two bodies are needed to define the position and orientation between the bodies. This is the kinematic arrangement utilized in Stewart Platforms which are commonly employed for flight simulators.

To minimize collection time, a six leg measurement procedure was utilized that was developed by John Ziegert [Kulkarni, 1996], see Appendix A. The only draw back to this procedure is the increased likelihood of bad measurement sensitivities in some coordinate directions. With care in the set-up, adequate sensitivity can be maintained. A sensitivity problem was encountered during early testing and was remedied by adding a 75 mm extension, in the -Z direction, to one of the tool sockets, Figure 5-1. To verify the accuracy of this set-up, angular parametrics were measured with both the nine and six leg techniques for comparison. The results were favorable, with only slight deviation, 3 arc-secs, between the methods for a few of the angular parametrics. The comparisons for the X axis angular parametrics are shown in Figure 5-2.

Keeping the collection time to a minimum is important to insure the errors are collected before significant thermal change can occur. The six leg measurement technique reduces the 21 parametric error data collection time from 20 to 13 minutes over the standard nine leg technique.

Data Collection Procedure

Data collection for a given thermal state begins with initialization of the LBB. Reinitializing before each measurement cycle minimizes thermal errors that can occur in

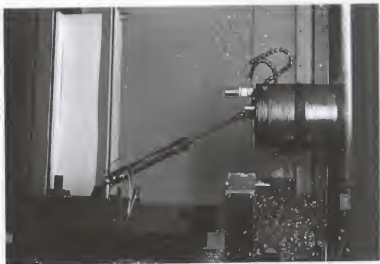


Figure 5-1 Measurement set-up for LBB error measurement on the machine.

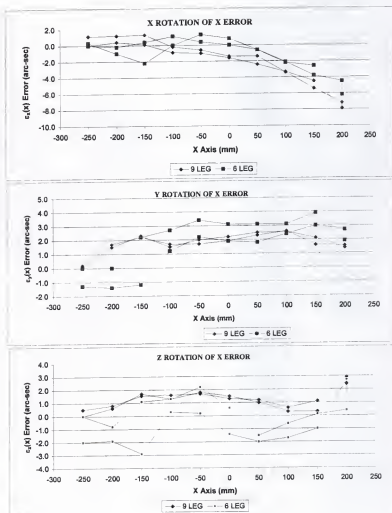


Figure 5-2 Error comparison between 6 and 9 leg technique.

in the LBB, see Appendix A. After initialization, the base lengths between the three sockets on the pallet are measured, Figure 5-1. Next the distances between the three sockets on the tool body are computed by trilaterating to each tool socket. The distance between each of the tool sockets is required for computing their location with the six leg measurement technique. Trilaterating to each tool socket is required to determine the distances between the tool sockets, since the LBB is too large to directly measure between them. The sockets are measured while the machine is at the commanded coordinate reference location, (0 280 340)mm. This coordinate reference is the position where all of the parametric errors are set to zero for the first measurement cycle. Comparing the position and orientation at this commanded location to that of the first measurement cycle provides the thermal displacement and orientation drifts.

Following these measurements, the six variable lengths are collected by running the machine through a measurement sequence six times. While the base lengths and tool positions can change over time, their variation is assumed to be negligible during a measurement cycle. Base length measurements were taken before and after a measurement cycle to verify this. Originally excessive growth was found in the I-Beam portion of the fixture, but was remedied by insulating it with 6 mm thick foam. Table 5-1 shows the base length measurement variations before and after a measurement cycle with and without insulation.

TABLE 5-1

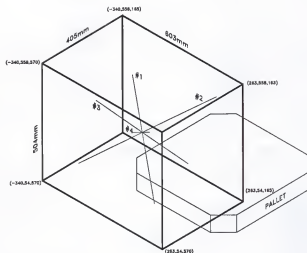
	LB1	LB2	LB3
NO INSULATION	2.35 μ m	4.17 μ m	4.43 μ m
INSULATED	0.35 μ m	1.35 μ m	1.52 μ m

The CNC program was repeatedly executed for each leg. Recording data for a single leg during a complete measurement sequence is referred to as sequential trilateration, see Appendix 1. The CNC program's commanded moves are as follows: The tool was moved from its start position (0 280 340)mm in the negative X direction -341.000 mm and then preloaded in the positive direction 1.000 mm. After a dwell of 0.5 seconds a relay was closed and then reopened to trigger a measurement from the LBB. One thousand laser readings were sampled at approximately 10 kHz and averaged to reduce vibrational noise. The machine was dwelled for 0.7 seconds to insure the data collection was complete. Next the machine was moved 67.000 mm in the positive X direction and the collection cycle (dwell-trigger-dwell-move) repeated. A total of nine moves in the positive direction were commanded. After the last positive move the axis was moved an additional 1.000 mm and then reversed 1.000 mm to preload the axis in the negative X direction. The data collection in the reverse direction was identical to that of the forward direction described above. At the completion of the X reversal measurements the machine was returned to its start position. Immediately following, a similar cycle was repeated for the Y axis with 56.000 mm steps and then for the Z axis with 45.000 mm steps. Each of the six variable legs were measured with this machine program. Measurement of the six legs took approximately 10 minutes. Parametric measurements over these ranges

combined with the HTM model resulted in a compensation volume of $603 \times 504 \times 405 \text{ mm}^3$, Figure 5-3.

Data Collection for Model Verification

The part machining tests evaluated the complete compensation system, but only over a limited amount of the compensated work space. To evaluate the models over a larger volume and verify their functionality before material is machined, body diagonals were measured with the LBB. Normally diagonal measurements are performed with a linear interferometer. However, alignment and set-up can be very time consuming. In order to further reduce the data collection time, only five points were measured bidirectionally along the diagonals. Diagonal measurements are a good evaluation of the whole model's functionality since all 21 parametric errors can contribute to their inaccuracy. Four body diagonals were measured at four different thermal states for each model: cold state-measure diagonals-30 minutes at 3500 RPM and 7 m/min all axes-measure diagonals-1 hour at 3500 RPM and 7 m/min all axes-measure diagonals-1 hour at 3500 RPM and 7 m/min all axes-1 hour cool down- measure diagonals. A spindle speed of 3500 RPM and 7 m/min axes actuation was chosen because it falls between the non-machining training cycles of 2500 RPM with 5 m/min and 5000 RPM with 10 m/min. Using the LBB did limit the diagonal measurement lines to 499 mm, 609 mm, 422 mm, and 394 mm. Figure 5-3 shows the body diagonals relative to the compensated work volume.



DIAGONALS:

- #1 $(-187.165, 430.257, 267.650)$ to $(144.945, 152.673, 490.709) = 498.607$ mm
 #2 $(-231.296, 144.857, 496.990)$ to $(183.855, 491.849, 218.157) = 608.688$ mm
 #3 $(-177.698, 422.344, 460.991)$ to $(144.945, 152.673, 490.709) = 421.550$ mm
 #4 $(-192.002, 177.700, 264.402)$ to $(76.459, 402.085, 444.711) = 393.613$ mm

Figure 5-3 Body diagonal's location relative to the compensation zone.

It should be noted that the compensation system implemented did not update the error coefficients in real time. The controller utilized did not permit real time updates. The coefficients were updated via an external computer using the controller's parallel port just before a CNC part program execution. For short programs such as the diagonal measurements and the B5.54 parts, this should not be a problem

Body Diagonal Measurement Procedure

First the coefficients were downloaded from the appropriate compensation model based on the temperature sensor readings taken from the external computer. Next the LBB was initialized and the three base lengths were measured. Then the LBB was placed between tool socket #1 and each of the three base sockets as the CNC program was sequentially executed three times for each length measurement, see Appendix A. Measurement of body diagonals 2, 3, and 4 followed, each requiring about 3.5 minutes to collect. The LBB was not reinitialized and the base lengths were not remeasured for the other body diagonals since the whole procedure could be completed in about 15 minutes.

B5.54 Part Machining Procedures

The ultimate test of any compensation system is to improve the accuracy of machined parts. Each of the compensation systems for this study were compared by machining the B5.54 precision positioning test part with compensation active at different thermal states, Figure 5-4. The part is intended to provide a statistically significant

number of features to test bidirectional positioning accuracy, repeatability, squareness, and circular profiling capability [ASME B5.54, 1992].

The test began by machining a part while the machine was in its cold state. Next the machine was warmed by machining scrap 6061 aluminum at a metal removal rate requiring 5 kW of energy for 8 minutes. Another B5.54 part was then machined at this new thermal state followed by a 1 hour cycle of 5000 RPM and 10 m/min spindle and axis actuation and then additional scrap machining requiring 10 KW for 4 minutes. A third B5.54 part was then machined. The machine was then allowed to cool, with all systems powered without actuation, for one hour. A final and fourth part was then machined at this cool down thermal state. This test cycle was performed with the machine tool control in its normal non-compensated mode and with the each of the 4 compensation systems active. Each model was evaluated with this test sequence on separate days with the ambient conditions held at nearly 24 °C before each test. Each part took approximately 30 minutes to machine including 10 tool changes. Approximately 285,120 mm³ of aluminum was removed from the part. Figure 5-5 and 5-6 show the scrap material and B5.54 part just prior to machining.

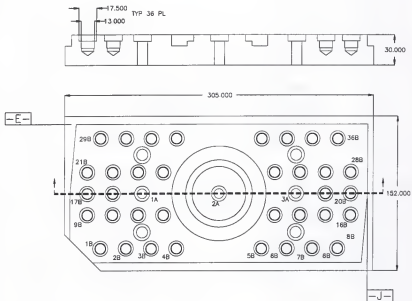




Figure 5-5 Scrap material just prior to machining.

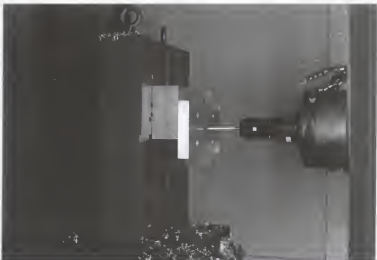


Figure 5-6 B5.54 test part just prior to machining.

CHAPTER 6 TEST RESULTS

Model Evaluations

The compensation models were evaluated for stability, accuracy, and post machine crash durability. Translational parametric errors (displacement and straightness) were measured over a four month period with 1st order thermal compensation active to evaluate stability. Body diagonals were measured with the LBB to evaluate accuracy improvements at different thermal states for all of the models. Test parts were also machined and inspected to evaluate all of the model's accuracy improvements at different thermal states. As the result of an accident, the durability of the models were tested after the tool was crashed into the tombstone.

Model Stability Evaluation

The durability of the geometric and thermal models is dependent on the stability of the machine's parametric errors. It is important that these errors remain constant over a long enough period so that remeasurement cycles can be minimized. Thermal duty cycle measurements with the LBB require a day to complete and manufacturers will certainly wish to minimize this non-machining use of their machines.

To evaluate the machine's geometric stability, parametric data were measured over a 4 month period. Correction data were collected on 8-20-97 and input into the controller. Translational parametric measurements were then taken over a 4 month period with the 1st order thermal created on 8-20-97 running inside the controller. Only the translational parametrics were examined because the angular parametrics can not be directly corrected without any rotary actuation capability. The translational parametrics were evaluated on the same lines in space along which compensation data was collected. During this 4 month period, the machine was used to machine a few miscellaneous parts, the B5.54 precision positioning part included, and some trial warm up tests involving spindle and axis actuation without machining. The amount of machine use would be considered light by industry standards. Figure 6-1, 6-2, and 6-3 compare the X, Y, and Z axis parametrics without compensation and with compensation over the 4 month period. The compensation is shown to be significant and stable over this time period. For instance, the $\delta y(X)$ error is reduced from about $24 \mu\text{m}$ to $3 \mu\text{m}$ and remains in this range throughout the 4 month period. Table 6-1 shows the axes squareness before compensation and after compensation for the 4 month period.

TABLE 6-1

Squareness Errors over 4 Month Period with Compensation (arc-secs)					
	No Comp	8-20-97	9-18-97	10-14-97	12-19-97
XY Squareness	7.5	-0.7	-0.1	0.4	2.2
XZ Squareness	-10.9	1.7	2.9	1.7	3.6
YZ Squareness	12.6	1.1	0.2	0.1	3.3

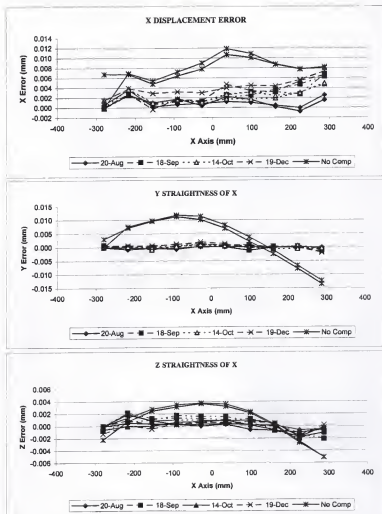


Figure 6-1 Compensated X-Axis translational parametrics over a 4 month period.

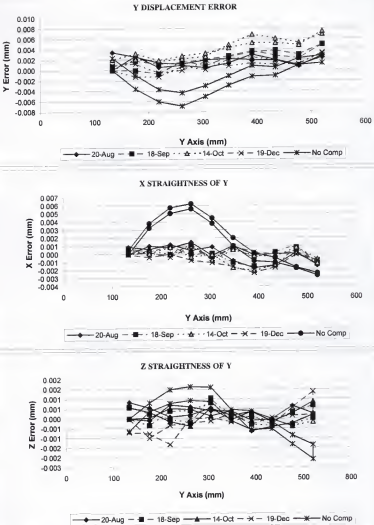


Figure 6-2 Compensated Y-Axis translational parametrics over a 4 month period.

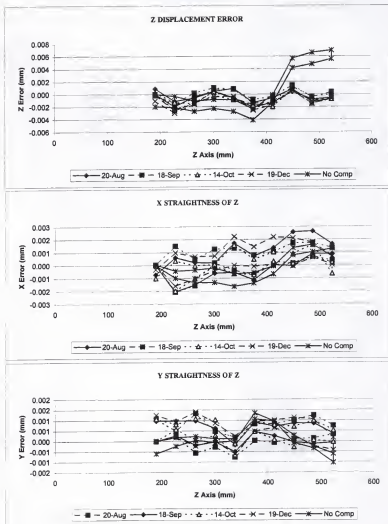


Figure 6-3 Compensated Z-Axis translational parametrics over a 4 month period.

Diagonal Measurement Evaluation of the Models

To evaluate the models over a larger volume than encompassed by the test parts and check for programming mistakes before wasting material, body diagonals were measured in the compensated work volume. The four body diagonals were measured at four different thermal states for each of the compensation systems with the LBB. Graphs for the first body diagonal at the four thermal states are shown in Figures 6-4 and 6-5. Table 6-2 shows the total ranges of the errors over all four thermal states and the improvement ratio over the uncompensated machine for each body diagonal.

TABLE 6-2

Diagonal Error Ranges over 4 Thermal States [microns][improve ratio]										
	No Comp		Geo Comp		1st Therm		ANN #1		ANN #2	
Diag #1	33.5	-	16.8	2.0	5.8	5.8	12.8	2.6	11.8	2.8
Diag #2	34.0	-	21.0	1.6	8.3	4.1	12.1	2.8	14.7	2.3
Diag #3	19.8	-	16.8	1.2	8.6	1.7	11.3	1.8	11.7	1.7
Diag #4	23.6	-	21.7	1.1	12.1	1.9	8.3	2.8	8.7	2.7

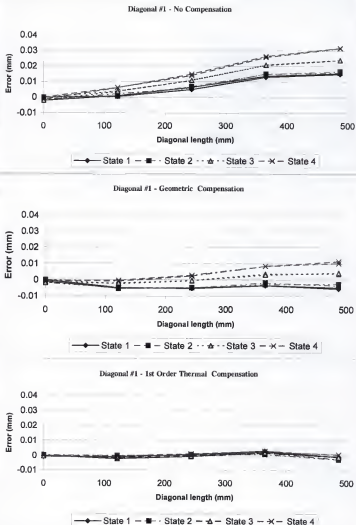
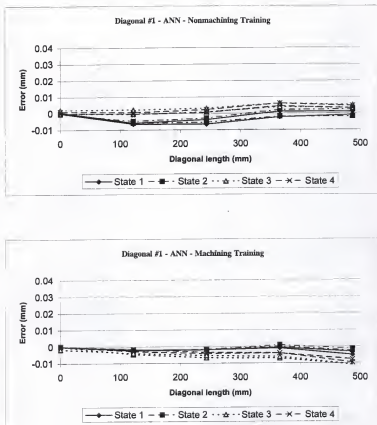


Figure 6-4 Body diagonal #1 for four thermal states: no compensation, geometric, and 1st order thermal.



Post Machine Crash Data

During data collection of the 5 kW machining training the face mill was accidentally crashed into the face of the tombstone between the 2nd and 3rd data collection runs. The crash occurred while the tool was approximately 50 mm from the tombstone as it was erroneously commanded into the tombstone via a Z axis rapid move. Five of the six carbide inserts were damaged absorbing much of the impact. Subsequent measurements showed a significant change in the linear portion of the straightness errors of the X and Z axis, specifically the $\delta x(Z)$ and $\delta z(X)$ errors, Figure 6-6. However the squareness between the X and Z axes did not significantly change, indicating the axes themselves remained unchanged. Observing the change in the first order terms of these two errors between the 2nd and 3rd runs revealed they changed by approximately the same magnitude, indicating that a rigid body rotation of the pallet locating interface must have occurred; change in $\delta z(X)$ term: -5.3 to -56.6 microns/meter, change in $\delta x(Z)$ term: 39.8 to 87.3 microns/meter. Subsequent measurements of these straightness errors showed that their coefficients were approximately the same as before the crash. Since this test required the removal of significant amounts of expensive aluminum, approximately \$800, it was not feasible to repeat it. Instead the appropriate first order coefficients were changed by 50 microns/meter to remove the rigid body rotation. This type of rigid body rotation would be significant and non removable if it occurred during the cutting of a part or if any part feature needed to be referenced to some feature on the pallet, such as a T-slot. However, for this research no features are machined that are dependent on any pallet reference.

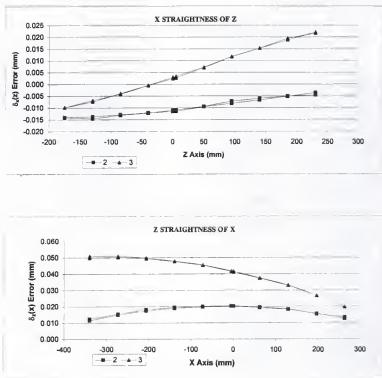


Figure 6-6 Change in straightness parametrics due to machine crash.

It is interesting to note that the parametric error coefficients lend themselves well for correction or modification of the model. This could be valuable if a machine crash revealed a change in alignment, because only a limited number of coefficients would require modification instead of remeasuring over an entire thermal state.

Machine Part Evaluation

The precision positioning test parts were inspected on a Brown and Sharpe Microval PFx CMM with an uncertainty of $\pm 0.002 \mu\text{m}$ in the plane of the measurements. The CMM was compensated in the plane of the part measurements and checked by measuring a fixed length (300 mm) ball bar at 6 different orientations in the plane.

Per the B5.54 standard, a coordinate system was defined relative to holes 1A, 2A, and 3A [ASME B5.54, 1992]. The bores and counter bores at locations 1B-36B were located by probing 6 points on their periphery to find a best fit circle, see Figure 5-4. The peripheral planes were probed at 54 and 11 locations for the X and Y surfaces, respectively. Table 6-3 through 6-6 compares the feature errors for the different models at the four thermal states. The features compared are: the X and Y positioning error for the bores and counter bores machined from the forward X and Y directions (locations 1B-18B) and reverse X and Y directions (locations 19B-36B); the XY squareness between surfaces -J- and -E-; and the X and Y dimensions between the peripheral surfaces. The errors reported for the bore and counter bores are given as the maximum, minimum, and span (max-min) of the 36 features. Circularity evaluations of the contouring cuts were inconclusive. A low pressure problem existed with the counter balance mechanism on the

TABLE 6-3

B5.54 Part Errors-Thermal State 1											
Feature Error		No Comp		Geo Comp		1st Thermal		ANN #1		ANN #2	
X (μm) Positioning FWD Bores & C-Bores 1B-18B	max	12.0	-	13.0	-	6.0	-	8.0	-	8.0	-
	min	-22.5	-	-23.8	-	-10.1	-	-17.8	-	-18.5	-
	span	34.5	-	36.8	0.9	16.1	2.1	25.8	1.3	26.5	1.3
Y (μm) Positioning FWD Bores & C-Bores 1B-18b	max	-1.1	-	-1.8	-	-2.3	-	-1.8	-	2.4	-
	min	-11.8	-	-13.7	-	-11.4	-	-10.6	-	-6.0	-
	span	10.7	-	11.9	0.9	9.1	1.2	9.3	1.2	8.4	1.3
X (μm) Positioning REV Bores & C-Bores 19B-36B	max	17.0	-	14.0	-	16.0	-	14.0	-	17.0	-
	min	-23.5	-	-24.2	-	-8.1	-	-20.9	-	-14.3	-
	span	40.5	-	38.2	1.1	24.1	1.2	36.9	1.2	31.3	1.3
Y (μm) Positioning REV Bores & C-Bores 19B-36B	max	-2.2	-	-3.3	-	0.4	-	11.6	-	0.5	-
	min	-12.3	-	-12.9	-	-5.5	-	-21.0	-	-7.2	-
	span	10.1	-	9.6	1.1	5.9	1.2	7.8*	1.2	7.7	1.3
XY Square arc-secs		-10.4	-	-13.3	0.8	7.2	0.5	19.8	0.5	32.4	0.3
X-DIM (μm)		18.1	-	16.2	1.1	56.8	0.3	35.9	0.5	43.3	0.4
Y-DIM (μm)		36.0	-	33.0	1.1	47.2	0.8	22.1	1.6	26.7	1.4

* Three outlier points excluded.

TABLE 6-4

B5.54 Part Errors-Thermal State 2											
Feature Error		No Comp		Geo Comp		1st Thermal		ANN #1		ANN #2	
X (μm) Positioning FWD Bores & C-Bores 1B-18B	max	13.0	-	0.0	-	0.0	-	16.0	-	14.0	-
	min	-23.8	-	-27.9	-	-13.4	-	-22.3	-	-25.1	-
	span	36.8	-	35.9	0.9	13.4	2.8	38.3	0.9	39.1	0.9
Y (μm) Positioning FWD Bores & C-Bores 1B-18B	max	1.8	-	0.2	-	4.3	-	5.9	-	2.3	-
	min	-13.7	-	-13.5	-	-19.0	-	-19.0	-	-11.4	-
	span	11.9	-	13.7	0.9	22.9	0.5	17.8	0.9	13.7	0.9
X (μm) Positioning REV Bores & C-Bores 19B-36B	max	14.0	-	21.0	-	15.0	-	22.0	-	21.0	-
	min	-24.2	-	-20.6	-	-6.8	-	-19.0	-	-23.0	-
	span	38.2	-	41.6	0.9	21.8	0.5	41.6	0.9	44.0	0.9
Y (μm) Positioning REV Bores & C-Bores 19B-36B	max	-3.3	-	-4.3	-	6.6	-	-4.3	-	-3.7	-
	min	-12.9	-	-10.3	-	-10.3	-	-12.7	-	-13.9	-
	span	9.6	-	11.1	0.9	16.9	0.6	15.8	0.6	10.2	0.9
XY Square arc-secs		-13.3	-	13.3	1.0	7.6	1.8	24.5	1.8	10.4	1.3
X-DIM (μm)		16.2	-	18.5	0.9	66.6	0.2	23.1	0.7	27.1	0.6
Y-DIM (μm)		33.0	-	33.2	1.0	51.8	0.6	29.3	1.1	21.3	1.6

TABLE 6-5

B5.54 Part Errors-Thermal State 3											
Feature Error		No Comp		Geo Comp		1st Thermal		ANN #1		ANN #2	
X (μm) Positioning FWD Bores & C- Bores 1B-18B	ma x	16.0	-	16.0	-	1.0	-	19.0	-	20.0	-
	mi n	-22.7	-	-25.5	-	-11.9	-	-20.9	-	-24.6	-
	spa n	38.7	-	41.5	0.8	12.9	0.8	39.9	0.9	44.6	1.1
Y (μm) Positioning FWD Bores & C-Bores 1B-18B	ma x	-4.4	-	1.0	-	-3.1	-	0.1	-	0.4	-
	mi n	-11.4	-	-11.4	-	-11.9	-	-13.6	-	-11.9	-
	spa n	9.9	-	12.4	0.8	15.9	0.9	13.7	0.8	15.9	0.6
X (μm) Positioning REV Bores & C-Bores 19B-36B	ma x	16.0	-	33.0	-	14.0	-	29.0	-	32.0	-
	mi n	-21.8	-	-21.8	-	-4.2	-	-17.2	-	-20.2	-
	spa n	38.7	-	54.7	0.8	46.2	0.8	46.2	0.8	52.2	1.1
Y REV (μm) Bores & C-Bores 19B-36B	ma x	-3.6	-	0.76	-	6.5	-	0.0	-	0.0	-
	mi n	-11.5	-	-10.9	-	-8.2	-	-13.2	-	-14.2	-
	spa n	7.9	-	11.6	0.7	14.7	0.5	13.2	0.6	14.2	0.6
XY Square arc-secs		-6.8	-	10.4	0.7	5.7	1.2	9.0	0.8	10.1	0.7
X-DIM (μm)		13.2	-	14.4	0.9	73.4	0.2	16.5	0.8	17.2	0.8
Y-DIM (μm)		37.6	-	32.1	1.2	56.2	0.7	28.1	1.3	19.1	2.0

TABLE 6-6

B5.54 Part Errors-Thermal State 4											
Feature Error		No Comp		Geo Comp		1st Thermal		ANN #1		ANN #2	
X (μm) Positioning FWD Bores & C-Bores 1B-18B	max	13.0	-	15.0	-	1.0	-	23.0	-	15.0	-
	min	-28.3	-	-28.3	-	-13.9	-	-28.3	-	-31.1	-
	span	37.3	-	14.8	0.6	14.8	2.5	51.3	0.7	16.1	0.7
Y (μm) Positioning FWD Bores & C-Bores 1B-18B	max	2.3	-	3.6	-	-0.2	-	-0.2	-	4.7	-
	min	-11.6	-	-13.9	-	-13.6	-	-13.9	-	-11.4	-
	span	13.9	-	21.7	0.7	18.4	0.8	13.7	0.6	16.1	0.7
X (μm) Positioning REV Bores & C-Bores 19B-36B	max	15.0	-	26.0	-	12.4	-	33.0	-	27.0	-
	min	-22.8	-	-13.9	-	-8.8	-	-26.2	-	-27.1	-
	span	37.8	-	45.8	0.6	21.7	0.8	59.2	0.6	54.1	0.7
Y (μm) Positioning REV Bores & C-Bores 19B-36B	max	-2.3	-	-1.6	-	5.8	-	-3.8	-	-1.3	-
	min	-11.6	-	-13.9	-	-8.8	-	-15.5	-	-15.5	-
	span	9.2	-	18.4	0.6	13.4	0.8	11.7	0.7	14.2	0.7
XY Square arc-secs		-14.4	-	16.9	1.3	16.9	0.9	11.5	1.3	14.8	0.9
X-DIM (μm)		15.2	-	11.6	1.3	70.1	0.3	4.2	3.6	12.1	1.3
Y-DIM (μm)		34.2	-	34.0	1.0	54.9	0.6	22.7	1.5	17.1	2.0

machine that caused unwanted vibrations at feed rates below 500 mm/min in the negative Y axis direction. This resulted in poor surface finish at the top and bottom of the milled reliefs in the center of the part, greatly overshadowing any potential improvements.

Examining the data reveals that only the 1st order thermal model showed significant improvement. The X positioning accuracy improved between 1.7 and 3.0 times over the non compensated part, similar to the diagonal test results. The Y axis positioning degraded as the machine was warmed, but the magnitude of the error span never exceeded 18.9 microns. The squareness error in general stayed the same magnitude or improved while changing sign from acute to obtuse. It should be noted that the accuracy of the squareness measurements is limited to about ± 4 arc-secs for a positional accuracy of $\pm 1.0 \mu\text{m}$ over the short Y axis surface of 50 mm. The only features to get substantially worse were the dimensions between the surfaces. The surfaces were very long (78 μm max), and this is unusual since all of the hole positions were slightly short (10 μm). This occurred, to a lesser extent, for all of the models. It is possible that the surface error was caused by either static or dynamic deflection of the tool. Down milling can be especially prone to undercutting since the forces tend to move the cutter away from the work piece. The hole locations would not be sensitive to tool deflection, only their size could be affected. The surface error was investigated by measuring the transfer function of the tool and inputting the cutting parameters into a simulation program to check for deflection, this is discussed in the next chapter.

The two neural network models only showed improvements at the cold state, improvement ratios of approximately 1.3. There appeared to be little difference between

them. Their accuracy deteriorated just below the accuracy of the non-compensated machine at the later thermal states. Their error was short, which is to be expected since the parts were machined at a higher temperature than 20 °C and this was not compensated for as in the 1st order thermal model. Additional cutting tests were conducted while the part temperature was monitored to correct for the part expansion. These tests are discussed in the next chapter.

CHAPTER 7

CONCLUSIONS AND RECOMMENDATIONS

The diagonal tests indicate that all of the models improved the machine's positioning accuracy. Unfortunately they all did not show significant improvement in the machining tests. Metal removal does add additional uncertainties that must be controlled to achieve similar results as in non-machining tests. However, machining accurate parts is the ultimate goal and function of a machine tool. Fortunately, the discrepancy is explainable, as subsequent testing proved.

In the following paragraphs, relevant conclusions are made from the data regarding the questions this research intended to investigate.

Success of Implementing Fuzzy ART-MAP on a Milling Machine

Previous research implemented the Fuzzy ART-MAP neural network on a 2-Axis lathe [Srinivasa, 1994]. The lathe network was trained using the volumetric errors at a grid of points in the 2D work zone as inputs. Implementing the network on 3-Axis machine, excluded measuring the volumetric errors as direct inputs into the network due to the order of magnitude increase in the number of points. Instead, as much of the deterministic solution was retained as possible, by using the kinematic model and allowing the network to predict its coefficients. This freed the network from having to determine the positional dependence of the errors, and focus on only their thermal dependence.

The diagonal tests showed that the network did a good job of reducing the errors at four different thermal states. Error reduction was on the order of 2-3X, maintaining the errors between about $\pm 5.5\mu\text{m}$ regardless of temperature. The 1st order thermal model performed slightly better, maintaining errors between about $\pm 4.0\mu\text{m}$. From translational parametric error measurements made after some of the diagonal tests, it appears the network's weakness was in its ability to accurately predict the displacement error variation with temperature. Given that only 24 thermal states were provided for training, the network performance was reasonable. This is an area where the deterministic approach is probably superior and adequate. Future researchers might consider combining the 1st order thermal compensation of the displacement errors with the neural network compensation of the remaining parametric errors.

At first glance, the data from the machining tests does not appear as favorable as the diagonal tests. But the apparent degradation in accuracy of the parts cut using the neural networks is explainable and expected. During the diagonal tests, the models are measured against the laser interferometer, which is compensated to be independent of temperature. During machining tests, the part material, unless cut at 20°C will affect the machined dimensions. The networks were designed to compensate the machine to be accurate, regardless of temperature, as the diagonal tests proved. The network produced parts improved the accuracy in the cold state, but appeared to degrade the accuracy at the later thermal states when compared to the non-compensated machined parts. This occurs, because as the machine warms, the atmosphere and part temperatures increase. The non-compensated scales expand with the part, helping to reduce the error, while the networks

attempt to maintain the scales at the same correct length. This has the effect of making the accuracy of the networks appear to degrade. Relative to a part's accuracy they do, but they are correctly positioning the machine. To be a more useful system, part temperature compensation should be added to the system as demonstrated in the 1st order thermal model. To verify what would be achievable with such a system, two additional parts were machined with network #2 and their part temperatures recorded to compensate out the part expansion error in the data. The results are shown in Table 7-1 and 7-2. As expected, the neural network compensated parts performed about as well as the 1st order thermal model. This is similar to the results from the diagonal tests. The surface distances are still too large, but this was found to be unrelated to the compensation models and is discussed below. In future work, performance might be improved if the 1st order and neural network models are combined.

Model Durability

The four month durability tests indicated that the 1st order thermal model maintained the machine's accuracy very well over this period. Squareness errors remained below 3.6 arc-secs and the translational parametric errors never exceeded a band of $\pm 5 \mu\text{m}$. During this four month period, a limited amount of machining occurred. As a final evaluation, the translational parametric errors were measured on 5-19-98 with the compensation data collected on 8-20-97, about a nine month period. During this period, all of the B5.54 parts and trial parts (approximately 30) were machined as well as about 67,000,000 mm³ of scrap material. The spindle unit was also replaced after the oil-mist

cooling and lubrication system quit, causing damage to the bearings. Also all 31 thermocouples were replaced prior to the final testing. The squareness errors and error ranges for the translational parametric errors

TABLE 7-1

B5.54 Part Errors-Thermal State 1									
Feature Error		No Comp		Geo Comp		1st Thermal		ANN #2 Temp Corrected	
X (μm) Positioning FWD Bores & C-Bores 1B-18B	max	12.0	-	13.0	-	6.0	-	0.9	-
	min	-22.5	-	-23.8	-	-10.1	-	-11.5	-
	span	34.5	-	16.1	2.1	16.1	2.1	12.4	2.8
Y (μm) Positioning FWD Bores & C-Bores 1B-18B	max	-1.1	-	-1.8	-	-2.3	-	0.2	-
	min	-11.8	-	-13.7	-	-11.4	-	-12.5	-
	span	10.7	-	11.9	1.2	9.1	1.2	12.7	0.8
X (μm) Positioning REV Bores & C-Bores 19B-36B	max	17.0	-	14.0	-	16.0	-	12.4	-
	min	-23.5	-	-24.2	-	-8.1	-	-3.3	-
	span	40.5	-	38.2	1.2	24.1	1.7	23.3	1.7
Y (μm) Positioning REV Bores & C-Bores 19B-36B	max	-2.2	-	-3.3	-	0.4	-	13.1	-
	min	-12.3	-	-12.9	-	-5.5	-	-7.3	-
	span	10.1	-	5.9	1.2	5.9	1.2	20.3	0.8
XY Square arc-secs		-10.4	-	-13.3	1.8	7.2	1.5	28.1	0.4
X-DIM (μm)		18.1	-	16.2	1.1	56.8	0.3	28.8	0.6
Y-DIM (μm)		36.0	-	33.0	1.1	47.2	0.8	16.9	2.1

TABLE 7-2

B5.54 Part Errors-Thermal State 3									
Feature Error		No Comp		Geo Comp		1st Thermal		ANN #2 Temp Corrected	
X (μm) Positioning FWD Bores & C-Bores 1B-18B	max	16.0	-	16.0	-	1.0	-	1.2	-
	min	-22.7	-	-25.5	-	-11.9	-	-13.0	-
	span	38.7	-	41.5	0.7	12.9	3.0	14.1	2.7
Y (μm) Positioning FWD Bores & C-Bores 1B-18B	max	-4.4	-	1.0	-	-3.1	-	-1.1	-
	min	-14.3	-	-11.4	-	-19.1	-	-19.1	-
	span	9.9	-	12.4	0.5	16.0	0.5	18.0	0.5
X (μm) Positioning REV Bores & C-Bores 19B-36B	max	16.0	-	33.0	-	14.0	-	15.2	-
	min	-21.8	-	-21.7	-	-4.2	-	0.1	-
	span	37.8	-	54.7	0.7	18.2	0.7	15.1	0.5
Y (μm) Positioning REV Bores & C-Bores 19B-36B	max	-3.6	-	0.76	-	6.5	-	7.6	-
	min	-21.8	-	-10.9	-	-8.2	-	-8.0	-
	span	7.9	-	41.5	0.7	13.2	0.5	13.6	0.5
XY Square arc-secs		-6.8	-	10.4	0.7	5.7	1.2	15.8	0.4
X-DIM (μm)		13.2	-	14.4	0.9	73.4	0.2	48.5	0.3
Y-DIM (μm)		37.6	-	32.1	1.2	56.2	0.7	40.9	0.9

are shown in Table 7-3. The XZ and YZ squareness errors have degraded to 6.4 and 5.2 arc-secs, respectively, but the XY squareness is still quite good, -0.7 arc-secs. All of the translational parametric errors remained at about the original compensation levels except for the X and Y displacement errors (10.5 and 10.9 μm). This could be caused by the replaced thermocouples. The 'T' type thermocouples only have an accuracy and repeatability of about 1.0 $^{\circ}\text{C}$. This would account for about 7.2 μm error in the X scale and about 6.0 μm in the Y scale measurements.

TABLE 7-3

Model Durability Follow-up Test						
	No Comp	8-20-97	9-18-97	10-14-97	12-19-97	5-19-98
XY (arc-sec)	7.5	-0.7	-0.1	6.1	2.2	-0.7
XZ (arc-sec)	-10.9	1.7	2.9	1.7	3.6	6.5
YZ (arc-sec)	12.6	1.1	0.2	0.1	3.3	5.8
$\delta x(X)$ (μm)	11.9	7.1	7.0	4.0	7.0	10.6
$\delta y(Y)$ (μm)	9.7	6.1	5.7	7.5	7.0	11.0
$\delta z(Z)$ (μm)	11.9	4.0	4.1	4.1	3.7	2.8
$\delta y(X)$ (μm)	25.3	4.0	2.1	2.1	4.1	5.8
$\delta z(X)$ (μm)	8.8	3.1	4.3	3.7	2.5	4.7
$\delta x(Y)$ (μm)	8.5	1.8	2.5	3.1	3.3	2.5
$\delta z(Y)$ (μm)	3.7	1.4	1.4	1.3	2.7	3.4
$\delta x(Z)$ (μm)	3.0	4.4	3.8	3.6	3.8	4.4
$\delta y(Z)$ (μm)	2.4	2.1	1.5	1.7	2.0	1.5

The technique of inputting the parametric errors into a rigid body model appears to be useful for error reduction over a 9 month period for this particular machine. How

well compensation durability translates to other machines will depend on the quality of their construction. It is reasonable to assume a machine with similar components would perform in a similar fashion.

Geometric vs. Thermal Modeling

Clearly the results of the diagonal and part tests reveal that geometric compensation only proves helpful at a single thermal state. The diagonal tests indicate that the geometric compensation reduced the errors at the cold state, but as soon as the machine was warmed, the accuracy deteriorated at the same rate as the uncompensated machine. In fact, due to the sign of the errors in the uncompensated cold state, as the machine warmed the uncompensated machine's accuracy improved for some of the diagonals, while the geometric compensated machine degraded. Geometric modeling might be adequate for scenarios in which the machine will be operated at or near a single thermal state such as the steady state reached in a long production run. However, thermal modeling must be considered if machines are to be used for flexible manufacturing, in which different numbers and types of parts are machined from day to day or week to week.

Deterministic vs. Non-deterministic Modeling

The first order thermal model utilized only deterministic methods. The volumetric error was computed from the parametric errors with a rigid body kinematic model. The displacement errors were modified according to scale temperature readings and published expansion coefficients. Only the thermal dependence of the remaining errors was not modeled. The neural network models also utilized the deterministic method of parametric

errors and rigid body modeling, but employed the non-deterministic ART-MAP's to model the parametric error variation with temperature.

From the diagonal measurements, the methods proved comparable, with the 1st order model fairing slightly better (improvement ratios of 4.1 vs. 2.8 were typical). From parametric measurements taken after each diagonal measurement, the neural network's weakness appeared to be in its inability to accurately model the displacement error variation with temperature. All of the other errors were reduced significantly. It is understandable that this occurred, since the displacement errors exhibited the largest change in shape with temperature. Each of the neural network models were only presented with 24 different thermal states for training. Assuming a typical variation in scale temperature over a thermal cycle to be on the order of 10°C, and an even distribution of these temperatures when measurements were taken, would at best produce 0.4 °C resolution. This is clearly inferior to a deterministic system capable of 0.1 °C resolution and it is unlikely the scale temperatures were evenly distributed..

An important feature provided by the 1st order thermal model was the ability to compensate the scales to the part material's temperature. This was not readily applicable to the neural networks since they would require additional training with different materials at different temperatures, greatly increasing the training time. The benefit of this feature is apparent in the machined part tests. The parts were machined at temperatures between 23-27°C and inspected at the international temperature standard of 20 °C. In the parts, this would be manifested in a shortness error of 26 µm at the maximum hole distance of 234 mm. In fact, the distance between the far holes were significantly short (approx. 25

μm) on all of the compensated parts, except those machined with the 1st order thermal compensation (approx. $10\mu\text{m}$). This attest to the importance of considering all sources of error, since any one might overshadow the mitigation of the others.

Thermal scale compensation is an area where deterministic methods are adequate and the non-deterministic methods do not appear to offer any substantial improvement.

Training with Machining vs. Non-machining

The two neural network models were identical in their architecture, but differed in their training cycles: one was trained with non-machining actuation for warm-up, and the other was trained with actual machining for warm-up. The diagonal tests did not reveal any clear preference. Over all the improvement ratios for the non-machining trained network were slightly better (2.6 to 2.8, 2.8 to 2.3, 1.8 to 1.7, and 2.8 to 2.7), however the diagonal tests were conducted with non-machine warm up.

During testing it was observed that the spindle housing reached much higher temperatures when not actually machining. Analysis revealed that this was not directly related to machining, but rather a related issue of whether coolant was or was not being used. The coolant is circulated through the spindle housing to jets directed at the tool. This forced convection cooling is most likely more significant to thermal distortion than the cutting process itself. Most of the cutting energy is transferred to the chip (approximately 80% at high cutting speeds) [Schey, 1987] which spends a short time in contact with the bed of the machine before being conveyed to a bin. The heat transfer from the chips to the bed will affect the bed temperature, but the lower mass spindle housing

combined with the large convective heat transfer is probably more significant contributor to thermal deformation. The greatest contribution of the chip removal is probably from its heat transfer to the coolant.

A secondary issue related to the coolant effect on the spindle housing and the LBB measurement procedure was observed. The X rotational errors were noticed to be larger for the non-machining tests. The spindle housing was suspected of large drifts during the measurement procedure as a result of the housing temperature rise. Drifting needs to be minimal during the measurement cycle for the measurements to be accurate with the LBB. The sequential measurement procedure relies on the assumption that the machine is in a quasi-stable state. To investigate this, the location of the tool sockets #1 and #2 were measured just after a 30 minute run of the spindle at 5000 RPM with the coolant off, followed by measurements 20 minutes later at the same commanded position. This is to simulate the conditions under which the non-machining measurements were taken. Table 7-4 shows the delta movement of the two sockets from just after warm-up to 20 minutes later.

TABLE 7-4

Socket Movement after 20 min dwell, following 30 min at 5000 RPM			
	$\Delta X(\mu\text{m})$	$\Delta Y(\mu\text{m})$	$\Delta Z(\mu\text{m})$
Socket #1	-15.2	0.0	33.0
Socket #2	-1.0	-20.0	34.0

The movements indicate that due to the rapid rise in temperature and low thermal mass, the spindle housing is contracting radially about 15 to 20 μm , and axially about 34

μm during the measurement cycle. This will distort the measurements taken with the LBB, especially the rotational errors since they rely on data taken over about a 15 minute cycle. The translational parametrics are collected in about 7 minutes and should be less affected. This contraction is less severe when the coolant is used, because it keeps the spindle from rising so much higher than the ambient temperature. Mounting to a fixture held in the spindle may have reduced the radial contraction, but not the axial. This was a surprising and unfortunate effect on the LBB measurement procedure. Fortunately the effect was not large enough to prevent satisfactory improvement of the machine's accuracy using the neural network models.

Metal Removal Testing vs. Non-machining Testing

This was not an intended topic of this research, but due to the discrepancy in the diagonal tests and the part machining tests for the neural network models, it seemed appropriate to discuss here. The diagonal measurement tests indicated that all three thermal models investigated improved the machines accuracy by a minimum improvement of about 2X. The B5.54 precision positioning tests only showed this kind of improvement for the 1st order thermal model. Also in all of the models, the surface to surface distance measurements were long while the bored hole spacings were short. Machining the parts at a higher temperature than 20°C explains the short dimensions, but not the large surface distances. This discrepancy was found to be partly caused by an incorrect tool diameter entered into the tool offset table. The nominal diameter of 12.000 mm was input into the table, subsequent measurements revealed that the actual diameter was 11.977 mm. This

error of 0.023 mm would cause the dimension across the surfaces to be larger by this amount. Cutting tests were conducted using the corrected tool diameter, see Table 7-1 and 7-2, but the surface distance still remained large by about 20-50 μm . Examination of the milling parameters revealed that the finishing cuts for these surfaces consisted of: 8.3% radial immersion, 11 mm depth of cut, down milling, 7000 RPM, and at a feed rate of 1310 mm/min. In down milling finishing cuts, forces can be present to move the cutter away from the surface of the part causing larger dimensions. The transfer function for this tool was measured and input into a simulation program to determine how much dynamic deflection would be expected based on the cutting parameters. The results are discussed below.

Surface Distance Error

Simulation tests on the tool deflection were inconclusive. The simulation was for a straight tooth cutter and showed excessively large deflections. To get a feel for the potential deflection magnitudes the static deflection can be computed. The static stiffness for a carbide cylindrical bar of 12 mm diameter at a tool length of 45 mm is 17,760 N/mm. The maximum cutting force per tooth obtained by integrating over the contact length of the helix is 256 N. This force would cause a deflection of 0.014 mm in the direction of the force. This force would not be normal to the cut surface, reducing the error effect. However the stiffness will probably be less than calculated due to imperfect and flexible clamping. With these considerations in mind, this calculation can still provide an estimate of the deflection. Such a deflection normal to the surface would account for

0.028 mm of the large dimension. This falls within the range of errors that were measured. Depending on the phasing of the tooth passing frequency and the tool's vibration this number could easily be larger since the dynamic stiffness is always smaller than the static stiffness. Regardless, the error most likely was caused by cutting deflection since the deflection insensitive boring operations did not reveal this type of positioning error.

As is evident from the testing, when conducting machining tests or machining actual parts, care must also be taken in controlling the machining parameters that affect accuracy. At these reduced levels of error, machine positioning improvement can be overshadowed by things such as cutter tolerance. Since precautions can be taken at the time of production to avoid these problems, positioning evaluation free of machining is still a satisfactory analysis tool. It provides valuable information about the machine itself, independent of user induced errors and dynamic effects.

Future Work

Further accuracy improvement might be achieved if the 1st order and neural network models would be combined. The 1st order model does a superior and satisfactory job of correcting the scale errors, but misses error variation such as changing squareness, which was observed in this study. Such a hybrid model might reduce the errors to within the $\pm 2.5 \mu\text{m}$ range. Also the use of the part material temperature compensation, which was not feasible on the neural network model, should be incorporated. The part material

sensor could probably be moved to the coolant bath to minimize its obtrusiveness in the work zone.

One goal of this study that was not achieved was implementation of a complete thermal model inside the controller of the machine. The computation limitations of the controller required an off-line external computer, limiting coefficient updates to just before part machining. This probably affected the accuracy of features machined at the end of the part cycle, 30 minutes, and would not be acceptable for longer cycle times. The 1st order thermal model was programmed into the controller, but problems with a peripheral thermocouple board prevented testing. An model running inside the controller with coefficient updates every minute would probably be sufficient.

Since the scale temperature proved to be such an important parameter for the error correction of the machine, it would probably be good to move the sensors from the housing to a place on the glass scale itself. This should eliminate any errors caused by differing time constants between the housing and scale.

Incorporating a thermal model in a commercial machine tool, with some of the improvements mentioned above, should allow the machine tool industry to make a similar accuracy leap that the CMM industry made 10 years ago for a small increase in cost.

APPENDIX A THE LASER BALL BAR

Background

Direct measurement of machine tool volumetric error to within micron accuracy at other than discrete points was not possible before the Laser Ball Bar. This capability allows for verification of a machine's geometric accuracy without machining test parts or making time consuming multiple parametric error measurements. Previously, each degree of error motion had to be measured with multiple instruments and set-ups and then combined in a kinematic model to compute the volumetric error.

From volumetric measurements taken with the LBB, the parametric errors can be decomposed as well. This multi degree error measurement capability from a single set-up greatly reduces data collection times over traditional instruments and techniques. Measuring the 21 parametric errors on a 3 axis machine takes under an hour with the LBB and at best 24 hours with other conventional instrumentation. Reducing this lengthy data collection time was the motivation that lead to the invention of the Laser Ball Bar.

The Instrument

The LBB is composed of a two stage telescopic assembly with precision spheres attached at the ends, Figure A-1. A heterodyne laser interferometer beam is carried to the instrument via a single mode polarization preserving fiber optic cable. The output from the fiber is collimated and passes through a 90R/10T non polarizing beam splitter. The 10% transmission beam passes through to a polarizer oriented at 45° for mixing of the two frequencies. This mixed beam then passes through a focussing optic for collection into a multimode fiber. The beat signal produced by mixing the two frequencies, taken after passage through the fiber optic cable, is used as the reference signal to eliminate cable induced phase shift errors [Yoshino, 1988]. The 90% reflected beam enters a polarization beam splitter, PBS, where the vertical polarization (f_1) is reflected and passes through a $\lambda/4$ wave plate to a retroreflector to make a second pass through the wave plate, rotating the polarization to pass back through the PBS. The horizontal polarization (f_2) passes through the PBS and a $\lambda/4$ plate and is directed down the hollow telescopic tubes to a retroreflector mounted in a fixture near the ball. The returned beam ($f_2 \pm \Delta f_2$) is Doppler shifted by the moving retroreflector and passes back through the $\lambda/4$ plate and reflects in the PBS to a focussing optic and 45° polarizer that combines the $f_2 \pm \Delta f_2$ and f_1 beams. This measurement beat signal is compared against the reference signal for computation of the retroreflector displacement.

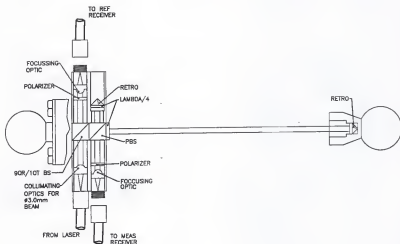


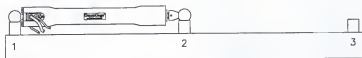
Figure A-1 Optical layout of the Laser Ball Bar.

Trilateration with the LBB

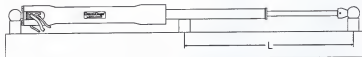
By itself, the LBB can only measure changes in length (displacement). To be used as a spatial measurement instrument, the absolute distance between sphere centers must be known. This is accomplished by utilizing its displacement measurement capability to provide a in-situ calibrated reference before every use, Figure A-2. The LBB is placed in a fixture with three collinear sockets spaced at a distance approximately equal to the minimum length of the LBB. The LBB is placed between the first two sockets and the interferometer is zeroed. Next the sphere in the second socket is extended to the third socket and the resulting displacement recorded. Finally the LBB is placed between the second and third sockets and the interferometer output is set to the previously recorded displacement. This transfer occurs in approximately 10 seconds, before the fixture can change length appreciably.

From this moment forward, the interferometer outputs the absolute distance between the sphere centers. This technique has the advantage of not requiring a precalibrated reference standard that must be maintained. All that is required of the fixture is that the sockets are collinear to within about ± 0.25 mm (± 0.010 in.).

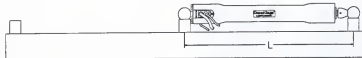
Because initialization is quick and easy, it can be performed as often as needed during a measurement procedure. Reinitializing often reduces any thermal drifting caused by material expansion between the spheres and optics [Mize, 1993].



STEP #1 THE LBB IS INITIALIZED TO ZERO



STEP #2 THE LBB IS EXTENDED FROM SOCKET 2 TO SOCKET 3
AND LENGTH L IS RECORDED



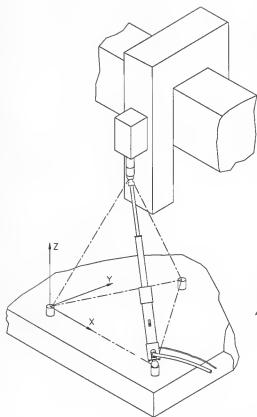
STEP #3 THE LBB IS INITIALIZED TO LENGTH L

Figure A-2 Initialization of the Laser Ball Bar.

Once initialized, the LBB is an extensible absolute length gage ready to be used for trilateration. Trilateration is a technique utilized in surveying and the Global Positioning Satellite system, GPS, in which the relative position between four points is determined from the six separating distances. The geometry and relevant equations are shown in Figure A-3.

For the LBB, the four points are realized by four spherical joints comprised of a magnetic socket containing trihedral supports for the spheres on the LBB. The three supports in the magnetic sockets produce a good spherical joint with a very little translation, $\pm 0.1 \mu\text{m}$ ($\pm 5.0 \mu\text{in}$) [Bryan, 1982].

On a machine tool, three of the magnetic sockets are placed on the work surface to provide a coordinate base. The fourth socket is attached to the body that carries the tool. In this way, the position of the tool is directly determined relative to the work surface. This is analogous to the arrangement in which the tool produces part features with respect to the raw material held on the work surface. With this set-up, machine tool volumetric positioning can be determined by comparing the LBB's trilaterated coordinates to the machine's commanded coordinates. For such a comparison to be meaningful, the commanded and measured coordinates must be expressed in the same system.



$$X = \frac{L_1^2 - L_2^2 + L_{B1}^2}{2L_{B1}}$$

$$C_1 = (L_1^2 - X^2)^{\frac{1}{2}}$$

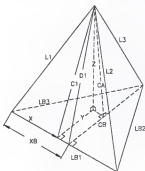
$$X_B = \frac{L_{B3}^2 - L_{B2}^2 + L_{B1}^2}{2L_{B1}}$$

$$C_B = (L_{B3}^2 - X_B^2)^{\frac{1}{2}}$$

$$D_1 = (C_1^2 + (X_B - X)^2)^{\frac{1}{2}}$$

$$Y = \frac{D_1^2 - L_3^2 + C_B^2}{2C_B}$$

$$Z = (C_1^2 - Y^2)^{\frac{1}{2}}$$



MEASURE 6 SIDES OF TETRAHEDRON
TO GET LOCATION OF TOOL WITH RESPECT
TO COORDINATE SYSTEM FORMED BY 3 BASE
SOCKETS ON MACHINE TABLE

Figure A-3 Geometry of trilateration.

Determining LBB to Machine Coordinate Transformation

The volumetric positioning data collected with the LBB is represented in a coordinate system based on the three base sockets. This coordinate system will most likely not be parallel to the machine's coordinate system. It is beneficial to know the measured coordinate positions in the machine's coordinate system. This is accomplished by measuring a rotation matrix between the LBB and machine coordinate system and then transforming the measured data.

Data collection for computing a rotation matrix consists of commanding the machine to move along two of its axes independently. For example: the machine is moved along its 'X' axis and paused at discrete points for trilateration with the LBB, see Figure A-4, followed by machine moves to discrete points along the 'Y' axis. Lines are fit by the method of least squares through these points. The best fit 'X' axis is vectorially crossed with the best fit 'Y' axis to obtain a perpendicular 'Z' axis. The 'Z' axis is then crossed with the 'X' axis to get a perpendicular 'Y' axis since the best fit 'Y' will not necessarily be perpendicular to 'X'. The direction cosines of these three machine axes described in the LBB system are the components that make up the rotation matrix between the two systems:

$${}^H R_B = \begin{bmatrix} l_x & m_x & n_x \\ l_y & m_y & n_y \\ l_z & m_z & n_z \end{bmatrix}$$

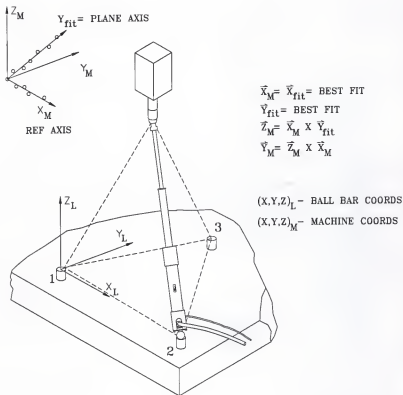


Figure A-4 Measuring a rotation matrix between the machine and LBB systems.

With this rotation matrix, data collected in the LBB system can be transformed into the machine's coordinate system.

Parametric Error Reduction from Coordinate Data

While direct volumetric data collection provides information nearest actual machining tests without actual machining, parametric error measurements can be more useful for diagnostics. Parametric errors can also be used in a kinematic model to obtain volumetric errors beyond the LBB's reachable work zone.

The reachable zone for the LBB is a volume bounded by the intersection of six spherical surfaces, a sphere of maximum and minimum LBB radius at each of the three base sockets. Parametric measurements obtained along the machine axes inside this work zone can be combined with a rigid body kinematic model to compute errors inside of a cube formed by the three axes. The errors computed within this cube are bounded by the normal limitations of rigid body modeling. This cube extends beyond the LBB's reachable work zone.

Trilateration of a single socket on the tool carrier, while the machine axes are commanded to move independently, provides the translative parametrics (displacement, and straightness) directly. To obtain the angular parametric errors of roll, pitch, and yaw, trilateration to an additional two tool sockets on the tool carrier body is required. The location of three non collinear points on a rigid body define its orientation and position. The angular parametrics are computed by taking the difference in the appropriate straightness or displacement errors between two of the tool sockets and dividing by the

appropriate component distance. For instance, the $\epsilon_x(y)$ error can be computed from either the $\delta x(y)$ deviation between two sockets divided by their Y component distance or the $\delta y(y)$ deviation between two sockets divided by their X component distance. The two sockets with the largest component separation are used for the computation to achieve the best measurement sensitivity.

Coordinate Error Sensitivity to Tetrahedron Geometry

Coordinate uncertainty is not only dependent on the uncertainty of the tetrahedron length measurements, but also on the nominal lengths of the tetrahedron. As the tetrahedron changes shape, the uncertainty of the individual coordinates will change even if the uncertainty of the individual lengths remains constant. This is easier to visualize if we consider a 2D computation. Figure A-5 shows a graphical description of 2D trilateration. The top picture shows a nearly equilateral triangle with arcs representing the uncertainty of L1 and L2. The uncertainty of measurement LB is not shown to simplify the figure. The uncertainty of the coordinates (x,y) is bounded in the region between the arcs. In the lower figure, the triangle is flattened, and for the same length uncertainty the 'y' coordinate accuracy is shown to significantly increase. This uncertainty can be determined mathematically by taking the partial derivatives of the coordinate equations with respect to the individual leg lengths. The coordinate accuracy is computed from a truncated Taylor series expansion. The equations for 3D error computation are as follows:

$$\delta X = \frac{\partial X}{\partial L_1} \delta L_1 + \frac{\partial X}{\partial L_2} \delta L_2 + \frac{\partial X}{\partial LB_1} \delta LB_1$$

$$\delta C_1 = \frac{\partial C_1}{\partial L_1} + \frac{\partial C_1}{\partial X} \delta X$$

$$\delta D_1 = \frac{\partial D_1}{\partial C_1} \delta C_1 + \frac{\partial D_1}{\partial X_B} \delta X_B + \frac{\partial D_1}{\partial X} \delta X$$

$$\delta C_B = \frac{\partial C_B}{\partial LB_3} \delta LB_3 + \frac{\partial C_B}{\partial X_B} \delta X_B$$

$$\delta X_B = \frac{\partial X_B}{\partial LB_3} \delta LB_3 + \frac{\partial X_B}{\partial LB_2} \delta LB_2 + \frac{\partial X_B}{\partial LB_1} \delta LB_1$$

$$\delta Y = \frac{\partial Y}{\partial D_1} \delta D_1 + \frac{\partial Y}{\partial L_3} \delta L_3 + \frac{\partial Y}{\partial C_B} \delta C_B$$

$$\delta Z = \frac{\partial Z}{\partial C_1} \delta C_1 + \frac{\partial Z}{\partial Y} \delta Y$$

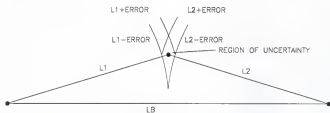
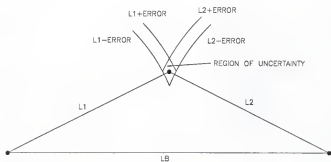


Figure A-5 Error sensitivity to trilateration geometry.

Instrument Accuracy

The LBB is capable of measuring coordinates in 3 dimensions with micron accuracy. Tests conducted at the Y-12 plant in Oak Ridge Tennessee on a Moore M-60 measuring machine, showed that the LBB measured 3D coordinates to within $\pm 0.4 \mu\text{m}$ over its measurement volume [Mize et al., 1994]. As discussed previously, the contributors of this error are a combination of the LBB's length error combined with the sensitivity of the geometry of the trilateration. The LBB's length error has several sources which will be described. There are eleven sources of error:

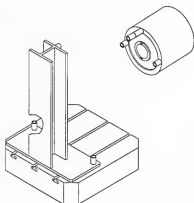
1. Uncompensated thermal deformation
2. Uncompensated elastic deformation
3. Axis misalignment to sphere centers
4. Cosine alignment of laser beam
5. Bending induced misalignment
6. Spherical joint translation
7. Initialization fixture misalignment
8. Wavelength compensation and dead path error
9. Laser Stability
10. Polarization Misalignment
11. Fiber optic path phase shifting

Errors 1 and 2 are caused by material length change between the optics and the sphere centers as a result of thermal and elastic deformation which is unsensed by the

interferometer. Errors 3, 4, and 5 are caused by misalignments of the laser path to shaft motions and the laser path to the line between the sphere centers. Error 6 results from unwanted translations caused by imperfections in the ball/socket spherical joint. Error 7 is caused by socket misalignment on the initialization fixture. Errors 8, 9, and 10 are common to all interferometer systems. Error 11 results from phase shifting caused by unequal optical paths along the two birefringent axis of a polarization maintaining fiber. This error has been eliminated in the current LBB design by taking the reference signal after passage through the fiber optic delivery cable as opposed to at the laser head [Yoshino, 1988]. These errors have been estimated and combined in an error budget for design purposes and to compute a theoretical length uncertainty. The arithmetic sum of these errors is 0.82 to - 0.89 μm and their root sum square is 0.50 to -0.51 μm . These numbers agree with the tests conducted at Oak Ridge [Mize et al., 1994]. For a more detailed description of these errors refer to [Mize, 1993].

Parametrics from Six Measurements

Trilaterating to three sockets on the moving body from three base sockets requires more measurements than is necessary to describe the position and orientation between the two bodies. For six degrees of freedom, only six measurements are required to constrain the system. This is analogous to a Stewart platform system in which six actuators position and orient a platform relative to a base platform. The measurement procedure is shown in Figure A-6. Other kinematic arrangements are possible.



MACHINE SET-UP

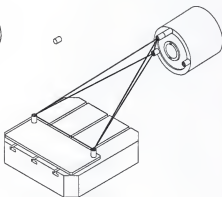
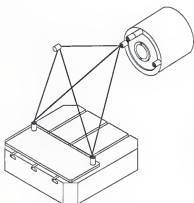
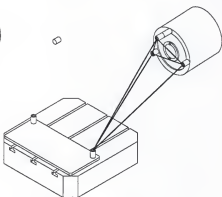
TRILATERATION TO
SECOND SOCKETTRILATERATION TO
FIRST SOCKETTRILATERATION TO
THIRD SOCKET

Figure A-6 Six leg measurement technique.

The measurement algorithm involves locating the two additional tool sockets relative to coordinate systems formed by three of the sockets that are not necessarily the base sockets. The first tool socket is still measured relative to the base sockets and the translational parametrics computed from these spatial coordinates. To locate the three tool sockets from six measurements, their separation distances need to be known. This could be accomplished by measuring between the sockets with LBB, in the same way the distances between the base sockets are measured, but their separation is generally less than the minimum LBB length. Instead the three tool sockets are located by trilateration from the base sockets at some arbitrary location prior to the six measurements. Their separation distances are computed by using the distance formula from their coordinate positions. Once the other two tool sockets have been located relative to a coordinate system based about three of the sockets, the transformation between these systems and the machine system are computed and used to transform their location into the machine's coordinate system. With the location of each tool socket known in the machine's coordinate system, the angular parametric errors can be computed as described previously.

APPENDIX B KINEMATIC MODEL IN CONTROLLER

The following code is for the function that computes the volumetric errors from the parametric error coefficients and the current machine position. The code is written in the 'C' language and resides inside the A950 controller of the machine.

```
static void ComputeComp(void){

    float  x, y, z;
    float  xTool, yTool, zTool;
    float  xTemperature, yTemperature, zTemperature;
    float  x2, x3, x4, y2, y3, y4, z2, z3, z4;
    float  exx, eyx, ezx, dxx, dyx, dzx;
    float  exy, eyy, ezy, dxy, dyy, dzy;
    float  exz, eyz, ezz, dxz, dyz, dzz;
    float  px, py, pz;
    float  ce;

    /* x, y, and z are in meters */
    x = ((float)PCD->proposed_cmd[LOG_X_AXIS]
        / INTERPS_PER_MM) / MM_PER_METER;
    y = ((float)PCD->proposed_cmd[LOG_Y_AXIS]
        / INTERPS_PER_MM) / MM_PER_METER;
    z = ((float)PCD->proposed_cmd[LOG_Z_AXIS]
        / INTERPS_PER_MM) / MM_PER_METER;

    if (Scratch_pad) { /* for debugging... */
        /* ints are in interp units */
        EXE_SCRATCH_PAD_INT[0] = PCD->proposed_cmd[LOG_X_AXIS];
```

```

EXE_SCRATCH_PAD_INT[1] = PCD->proposed_cmd[LOG_Y_AXIS];
EXE_SCRATCH_PAD_INT[2] = PCD->proposed_cmd[LOG_Z_AXIS];
/* floats are in millimeters */
EXE_SCRATCH_PAD_FLOAT[0] = x * MM_PER_METER;
EXE_SCRATCH_PAD_FLOAT[1] = y * MM_PER_METER;
EXE_SCRATCH_PAD_FLOAT[2] = z * MM_PER_METER;
}

/* get the current tool length */
zTool = Tool_length;

if (UseTemperature)
{
    xTemperature = temperatures[xInput];
    yTemperature = temperatures[yInput];
    zTemperature = temperatures[zInput];
    ce = coef_expan;
}
else
{
    xTemperature = 0.0;    // until temperature is included
    yTemperature = 0.0;    // set values to zero, so they
    zTemperature = 0.0;    // are not included in the
    ce = 0.0;              // calculations.
}

x -= x0; //normalize coordinates to intersection point(x0,y0,z0)
y -= y0;
z -= z0;

xTool = xTool0;    // get tool offsets
yTool = yTool0;
zTool -= zTool0;

x2 = x*x;
x3 = x2*x;
x4 = x3*x;
y2 = y*y;
y3 = y2*y;
y4 = y3*y;
z2 = z*z;
z3 = z2*z;

```



```
z4 = z3*z;
```

```
// polynomials of X axis parametric errors
exx = a4*x4 + a3*x3 + a2*x2 + a1*x;
eyx = b4*x4 + b3*x3 + b2*x2 + b1*x;
ezx = c4*x4 + c3*x3 + c2*x2 + c1*x;
dxx = d4*x4 + d3*x3 + d2*x2 + d1*x +
      ce*(xTemperature-xTemp0)*x;
dyx = e4*x4 + e3*x3 + e2*x2 + e1*x;
dzx = f4*x4 + f3*x3 + f2*x2 + f1*x;

if (x < X_previous) /* if negative direction, include */
{ /* the 0 coefficients */
    exx += a0;
    eyx += b0;
    ezx += c0;
    dxx += d0;
    dyx += e0;
    dzx += f0;
}
```

```
//polynomials for Y axis parametric errors
exy = g4*y4 + g3*y3 + g2*y2 + g1*y;
eyy = h4*y4 + h3*y3 + h2*y2 + h1*y;
ezy = i4*y4 + i3*y3 + i2*y2 + i1*y;
dxy = j4*y4 + j3*y3 + j2*y2 + j1*y;
dyy = k4*y4 + k3*y3 + k2*y2 + k1*y +
      ce*(yTemperature-yTemp0)*y;
dzy = l4*y4 + l3*y3 + l2*y2 + l1*y;
if (y < Y_previous) /* check negative direction */
{
    exy += g0;
    eyy += h0;
    ezy += i0;
    dxy += j0;
    dyy += k0;
    dzy += l0;
}
```

```
//polynomials for Z axis parametric errors
```

```

exz = m4*z4 + m3*z3 + m2*z2 + m1*z;
eyz = n4*z4 + n3*z3 + n2*z2 + n1*z;
ezz = o4*z4 + o3*z3 + o2*z2 + o1*z;
dxz = p4*z4 + p3*z3 + p2*z2 + p1*z;
dyz = q4*z4 + q3*z3 + q2*z2 + q1*z;
dzz = r4*z4 + r3*z3 + r2*z2 + r1*z +
      ce*(zTemperature-zTemp0)*z;
if (z < Z_previous) /* check negative direction */
{
  exz += m0;
  eyz += n0;
  ezz += o0;
  dxz += p0;
  dyz += q0;
  dzz += r0;
}

// volumetric error equations
px = -dxx - dxy - dxz +
      y * (ezz + ezx) +
      yTool * (ezx + ezy + ezz + ez0) -
      zTool * (eyx + eyy + eyz + ey0) - ccx;

py = -dyy - dyy - dyz -
      x * ezz -
      xTool * (ezx + ezy + ezz + ez0) +
      zTool * (exx + exy + exz + ex0) - ccy;

pz = -dzz - dzy - dzz +
      x * eyz - y * (exz + exx) +
      xTool * (eyx + eyy + eyz + ey0) -
      yTool * (exx + exy + exz + ex0) - ccz;

/* px, py, and pz are in microns, geometric_comps are in interp units
*/
PCD->geometric_comp[LOG_X_AXIS] = (int_32)(px *
GEOMETRIC_COMP_SCALE);
PCD->geometric_comp[LOG_Y_AXIS] = (int_32)(py *
GEOMETRIC_COMP_SCALE);
PCD->geometric_comp[LOG_Z_AXIS] = (int_32)(pz *
GEOMETRIC_COMP_SCALE);

if (Scratch_pad) { /* for debugging... */

```

```

        /* ints are in interp units */
EXE_SCRATCH_PAD_INT[3] = PCD->geometric_comp[LOG_X_AXIS];
EXE_SCRATCH_PAD_INT[4] = PCD->geometric_comp[LOG_Y_AXIS];
EXE_SCRATCH_PAD_INT[5] = PCD->geometric_comp[LOG_Z_AXIS];
        /* floats are in millimeters */
EXE_SCRATCH_PAD_FLOAT[3] =
    (px * GEOMETRIC_COMP_SCALE) / INTERPS_PER_MM;
EXE_SCRATCH_PAD_FLOAT[4] =
    (py * GEOMETRIC_COMP_SCALE) / INTERPS_PER_MM;
EXE_SCRATCH_PAD_FLOAT[5] =
    (pz * GEOMETRIC_COMP_SCALE) / INTERPS_PER_MM;
    }

X_previous = x;      /* save for direction check */
Y_previous = y;
Z_previous = z;

```

```

}

```

APPENDIX C

PARAMETRIC ERROR MEASUREMENT DATA

The following graphs show the parametric data collected for the model training. The axis coordinates are the normalized coordinates used for the compensation system, (0,0,0) in the compensation system corresponds to (0280,340) in the machine system. The drift of each of the errors is included in the graphs. The straightness data includes the squareness errors.

The cold state data from the 5000 RPM non machining thermal cycle was used for the geometric and 1st order thermal compensation models. In the Z straightness of X and X straightness of Z data collected during 5 kW thermal cycle, notice the change in the slopes after the 2nd runs due to a rigid body rotation caused by the machine crash discussed in chapter 6. All of the data was collected with the LBB over 4 separate days.

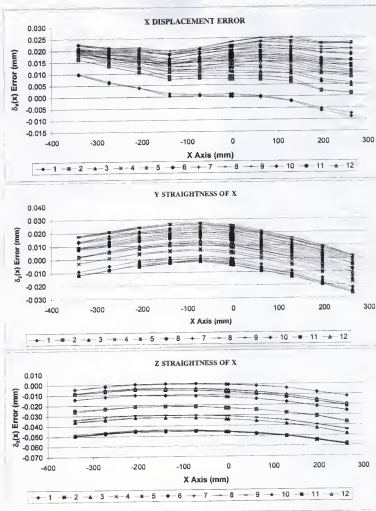


Figure C-1 X-Axis translational parameters for 2500 RPM - 5 m/min thermal cycle.

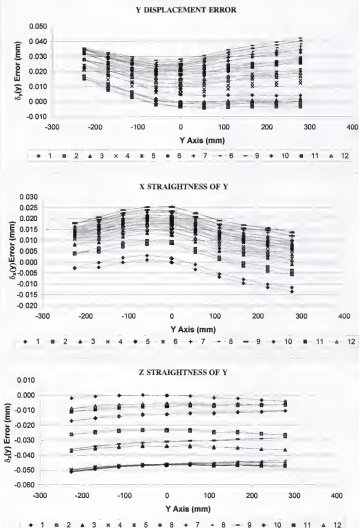


Figure C-2 Y-Axis translational parametrics for 2500 RPM - 5 m/min thermal cycle.

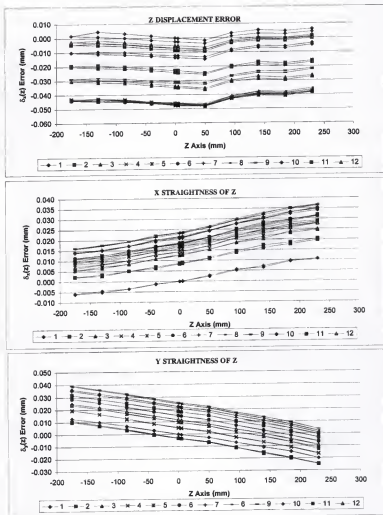


Figure C-3 Z-Axis translational parameters for 2500 RPM - 5 m/min thermal cycle.

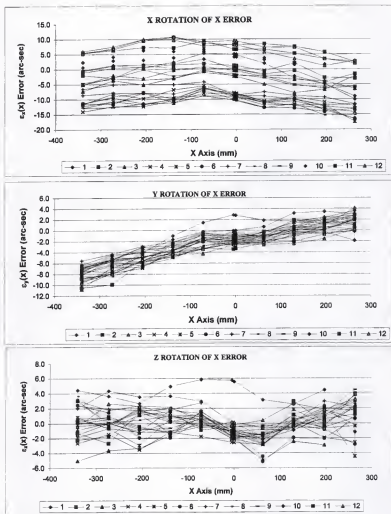


Figure C-4 X-Axis angular parameters for 2500 RPM - 5 m/min thermal cycle.

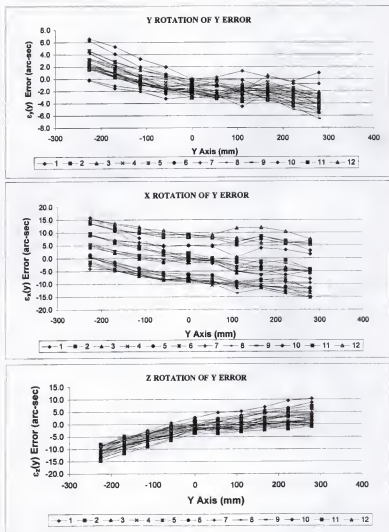


Figure C-5 Y-Axis angular parametrics for 2500 RPM - 5 m/min thermal cycle.

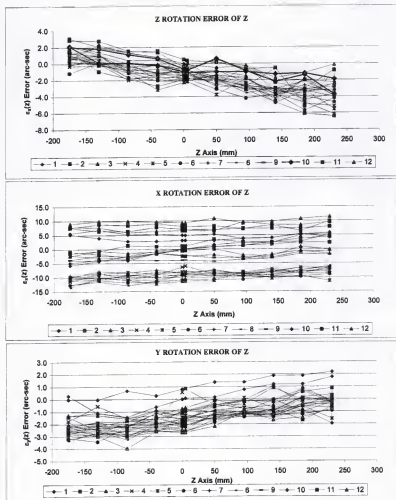


Figure C-6 Z-Axis angular parameters for 2500 RPM - 5 m/min thermal cycle

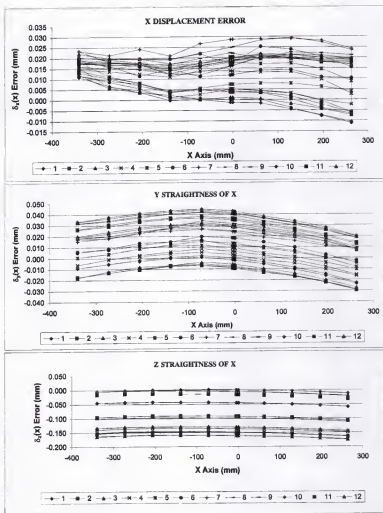


Figure C-7 X-Axis translational parametrics for 5000 RPM - 10m/min thermal cycle.

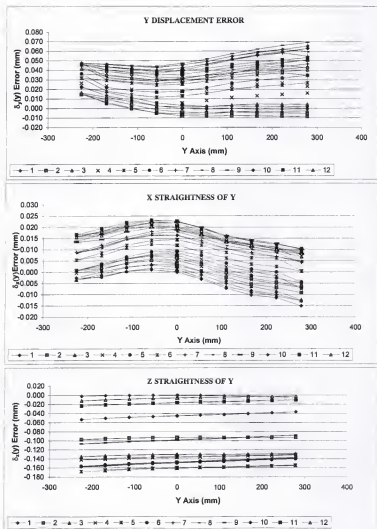


Figure C-8 Y-Axis translational parameters for 5000 RPM - 10 m/min thermal cycle.

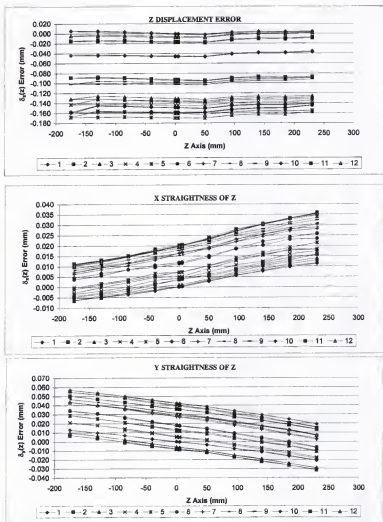


Figure C-9 Z-Axis translational parameters for 5000 RPM - 10 m/min thermal cycle.

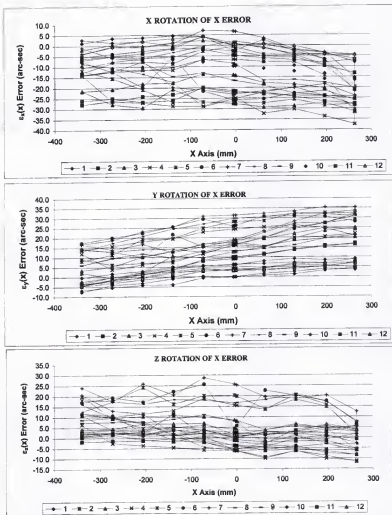


Figure C-10 X-Axis angular parameters for 5000 RPM - 10 m/min thermal cycle.

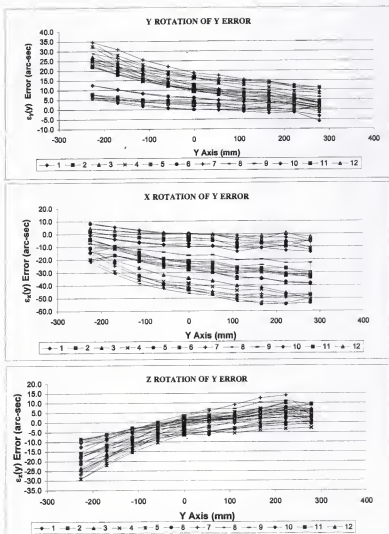


Figure C-11 Y-Axis angular parametrics for 5000 RPM - 10 m/min thermal cycle.

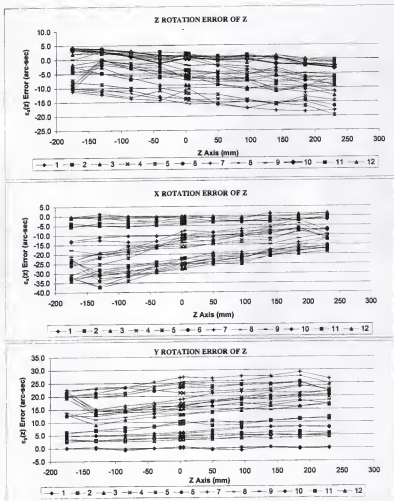


Figure C-12 Z-Axis angular parametrics for 5000 RPM - 10 m/min thermal cycle.

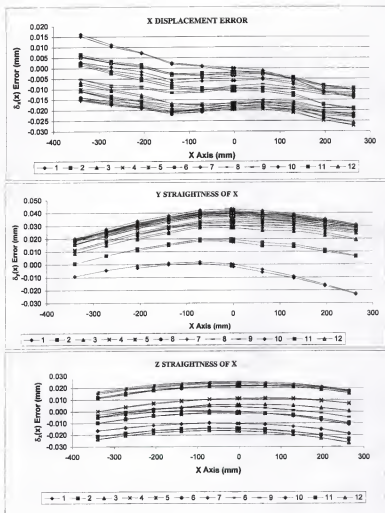


Figure C-13 X-axis translational parameters for 1 kW machining thermal cycle.

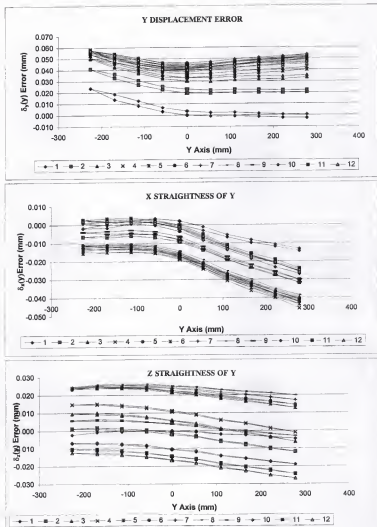


Figure C-14 Y-Axis translational parametrics for 1 kW machining thermal cycle.

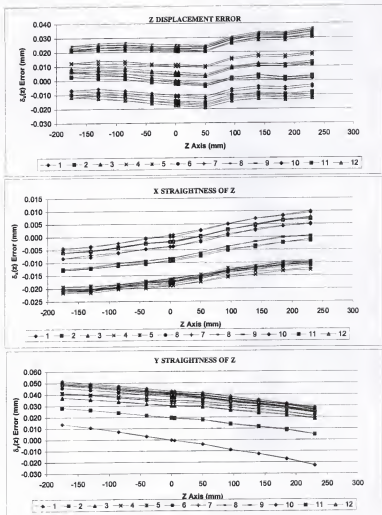


Figure C-15 Z-Axis translational parametrics for 1 kW machining thermal cycle.

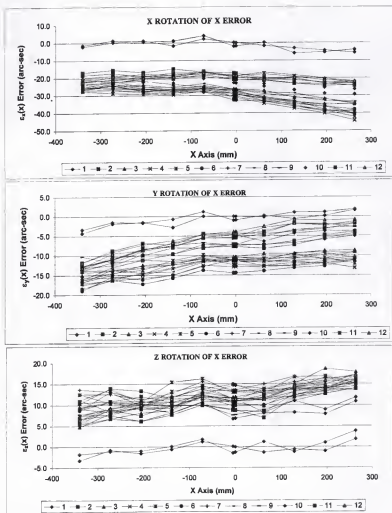


Figure C-16 X-Axis angular parametrics for 1 kW machining thermal cycle.

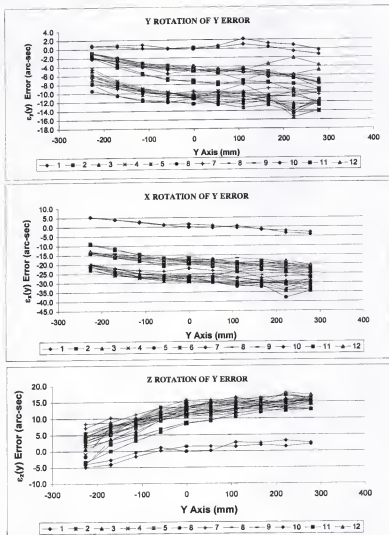


Figure C-17 Y-Axis angular parametrics for 1 kW machining thermal cycle.

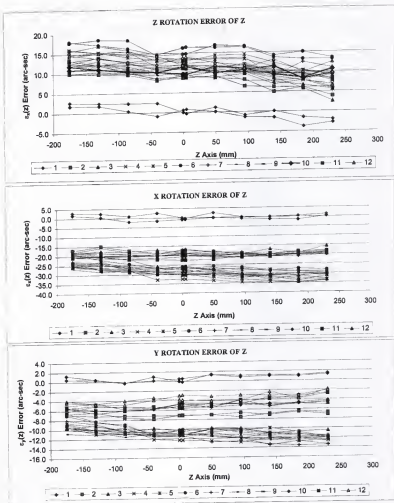


Figure C-18 Z-Axis angular parametrics for 1 kW machining thermal cycle.

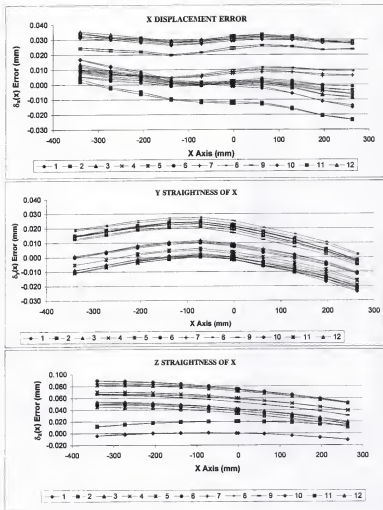


Figure C-19 X-Axis translational parametrics for 5 kW machining thermal cycle.

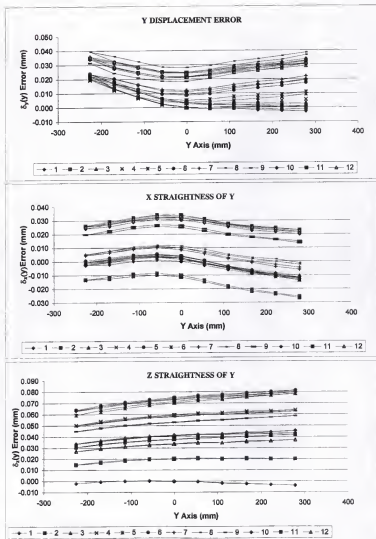


Figure C-20 Y-Axis translational parametrics for 5 kW machining thermal cycle.

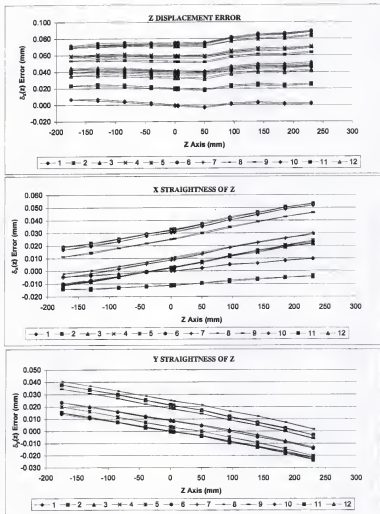


Figure C-21 Z-Axis translational parametrics for 5 kW machining thermal cycle.

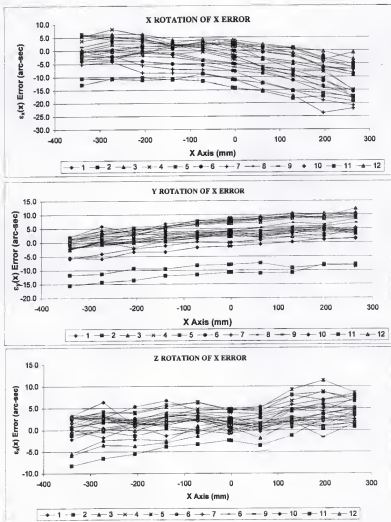


Figure C-22 X-Axis angular parametrics for 5 kW machining thermal cycle.

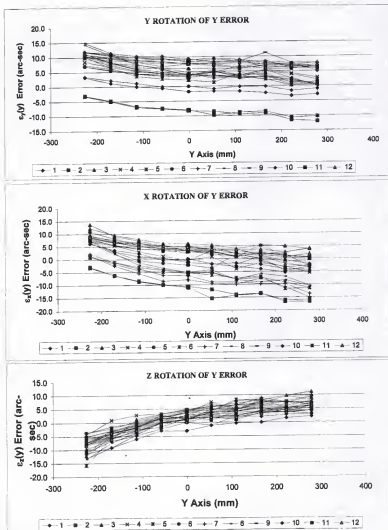


Figure C-23 Y-Axis angular parametrics for 5 kW thermal cycle.

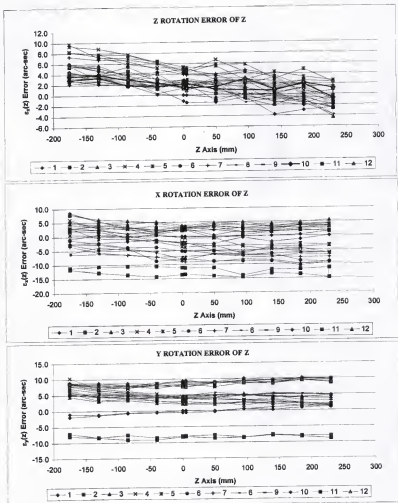


Figure C-24 Z-Axis angular parametrics for 5 kW machining thermal cycle.

LIST OF REFERENCES

- Allen, J. P., Postlethwaite, S. R., Ford, D. G., "Practical Thermal Error Correction for CNC Machine Tools," ASPE Proceedings, vol. 14, pp. 648-653, 1996.
- Aronson, R. B., "New Waves in Manufacturing: A Bright Horizon for Machine Tool Technology," Manufacturing Engineering, vol. 116/No. 3, pp. 57-70, 1996.
- Aronson, R. B., "Hexapods: Hot or Ho-Hum," Manufacturing Engineering, vol. 119/No. 4, pp. 60-67, 1997.
- ASME B5.54, "Methods for Performance Evaluation of Computer Numerically Controlled Machining Centers," New York, NY, 1992.
- Balsamo, A., Marques, D., Sartori, S., "A Method for Thermal-Deformation Corrections of CMMs," CIRP Annals, 1990.
- Blaedel, K. L., "Error Reduction," Technology of Machine Tools, Volume 5: Machine tool Accuracy. University of CA, Livermore, UCRL-52960-5, October 1980.
- Bryan, J. B., "International Status of Thermal Error Research," CIRP Annals, Vol 16, pp. 203-215 1968.
- Bryan, J. B., "Design and Construction of an 84-inch Diamond Turning Machine," Precision Engineering vol. 1, pp. 13-17, 1979.
- Bryan, J. B., "A Simple Method for Testing Measuring Machines and Machine Tools," Precision Engineering, vol. 4/2, pp. 61-69, 1982.
- Bryan, J. B., "International Status of Thermal Error Research," CIRP Annals, vol. 39/2, pp. 645-656, 1990.
- Carpenter, G. A., Grossberg, S., Rosen, D. B., "Fuzzy ART: Fast Stable Learning and Categorization of Analog Patterns by an Adaptive Resonance System," Neural Networks, vol. 4, pp. 759-771, 1991.

- Chen, J. S., "Real-Time Compensation of Time-Variant Volumetric Error on a Machining Center," Ph.D. Dissertation, University of Michigan, Ann Arbor, 1991.
- Denavit, J., Hartenberg, R. S., "A Kinematic Notation for Lower Pair Mechanisms Based on Matrices," *ASME Journal of Applied Mechanics*, pp. 215-221, June 1955.
- Donmez, M. A., "A General Methodology for Machine Tool Accuracy Enhancement: Theory, Application and Implementation," Ph.D. Dissertation, Purdue University, West Lafayette, 1985.
- Estler W. T., Magrab, E. B., "Validation Metrology of the Large Optics Diamond Turning Machine," National Bureau of Standards, Gaithersburg, MD, NBSIR 85-3182(R), June 1985.
- French, D., Humphries, S. H., "Compensation for the Backlash and Alignment Errors in a Numerically Controlled Machine Tool by a Digital Computer Programme," *MTDR*, 1967.
- Hocken, R. J., "Technology of Machine Tools," *UCRL-52960-5*, vol. 5, 1980.
- Hocken, R. J., Simpson, J. A., Borchardt, B., Lazar, J., Reeve, C., Stein, P., "Three Dimensional Metrology," *Annals of the CIRP*, vol. 26/2, pp. 403-408, 1977.
- Huang, P.S., Li, Y., "Laser Measurement Instrument for Fast Calibration of Machine Tools," *ASPE Proceedings*, vol. 14, pp. 644-647, 1996.
- Janeczko, J., "Machine Tool Thermal Distortion Compensation," *NMTBA (4th Bienn. International Machine Tool Technology Conference)*, 1988.
- Koda, Seido, Ushio, Yoshihiro, "Development of the Automatic Measurement Correction System for Machining Centers - High Accuracy Positioning Working," *Bulletin Japan Society of Precision Engineering*, 1981.
- Krulwich, D., Hale L., Yordy D., "Rapid Mapping of Volumetric Errors," *ASPE Proceedings*, vol. 12, pp. 408-411, 1995.
- Kulkarni, R. "Design and Evaluation of a Technique to Find the Parametric Errors of a Numerically Controlled Machine Tool Using a Laser Ball Bar," Master's Thesis, University of Florida, Gainesville, 1996.
- Leete, D. L., "Automatic Compensation of Alignment Errors in Machine Tools," *International Journal of MTDR*, vol. 1, 1961.

- Ma, Q., Chu, X., Lau, K., "A 5-Degree-of-Freedom Laser System for Rapid Machine Volumetric Error Measurement and Compensation," ASPE Proceedings, vol. 14, pp. 642-643, 1996.
- McClure, E. R., "Manufacturing Accuracy Through the Control of Thermal Effects," Ph.D. Dissertation, Lawrence Livermore National Laboratory, Livermore, CA, UCRL-50636, 1969.
- Mize, C. D., "Design and Implementation of a Laser Ball Bar Based Measurement Technique for Machine Tool Calibration," Master's Thesis, University of Florida, Gainesville, 1993.
- Mize, C. D., Ziegert, J. C., Pardue, R., Zurcher, N., "Spatial Measurement Accuracy Tests of the Laser Ball Bar" Final Report for CRADA No. Y-1293-0224 between Martin Marietta Energy Systems and Tetra Precision Inc., August 1994.
- NIST-60NANB2D1214, "Software Correction of Precision Machines," Gaithersburg, MD, July 1993.
- Okushima, K., Kakino, Y., Higashimoto, A., "Compensation of Thermal Displacement by Coordinate System Correction," CIRP Annals, 1975.
- Schede, R. W., "Automatic Error Correction Permits Conversion of 66 Inch Boring Mill Into Precise Inspection Machine," MTDR, 1967.
- Schlesinger, G., Inspection Tests on Machine Tools, 1927; latest edition is Testing Machine Tools, 8th ed., revised by F. Koenigsberger and M. Burdekin Pergamon Press, New York 1978.
- Schey, John A, Introduction to Manufacturing Processes, Second Edition McGraw-Hill Inc., New York 1987.
- Schultschik, R., "The Components of the Volumetric Accuracy," CIRP Annals, vol. 25/1 pp. 223-227, 1977.
- Shuhe, L., Zhang, Y., Zhang, G., "A Study of Pre-Compensation for Thermal Errors of NC Machine Tools," International Journal of Machine Tools & Manufacture, (accepted for publication), 1997.
- SIP (Societe Genevoise, d'Instruments de Physique), As Ninety Years Went By..., Geneva, Switzerland, 1952.
- Soons, H. A., Simone, L. Y., "Precision in Machining: Research Challenges," NISTIR

5628, U.S. Department of Commerce, Gaithersburg, MD, May 1995.

Srinivasa, N., "Modeling and Prediction of Thermally Induced Errors in Machine Tools Using a Laser Ball Bar and a Neural Network," Ph.D. Dissertation, University of Florida, Gainesville, 1994.

Srinivasa, N., Ziegert, J. C., Smith, S., "Prediction of Thermal Errors in Machine Tools Using Artificial Neural Networks," Proceedings of NSF Design and Manufacturing Systems Conference, Charlotte, NC, pp. 1725-1732, 1993.

Sumanth, D., "Implementation of a Real-Time Error Compensation System on a CNC Turning Center," Master's Thesis, University of Florida, Gainesville, 1993.

Teeuwssen, J.W.M.C., Soons, J. A., Schellekens, P.H.J., "A General Method for Error Description of CMMs Using Polynomial Fitting Procedures," CIRP Annals, vol. 38/1, pp. 505-510, 1989.

Thusty, J., "Techniques for Testing Accuracy of NC Machine Tools," 12th MTDR Conf., pp.333-345, 1971.

Thusty, J., "Testing of Accuracy of NC Machine Tools," Report No. UCRL-52960-Supp. 1, 1980.

Thusty, J., and Mutch, G.F., "Testing and Evaluating Thermal Deformations of Machine Tools," Proceedings of the 14th MTDR Conference, pp. 285-297, 1973.

Venugopal, R., and Barash, M., "Thermal Effects on the Accuracy on Numerically Controlled Machine Tools," CIRP Annals, vol. 35/1, pp. 255-258, 1986.

Wasiukiewicz, I., "The Improvement in Accuracy of High Precision Machine Tools by Means of Adaptive Control," 15th MTDR Proc., 1974.

Wong, G.S.K., Koenigsberger, F., "Automatic Correction of Alignment Errors in Machine Tools," International Journal of Machine Tool Design Research, vol. 6, 1967.

Yoshino, T., "Heterodyne Technology for Optical Sensors," Optical Fiber Sensors, vol. 2 part 1, pp. 40-43, January 1988.

Ziegert, J., "Measurement of Machine Tool Parametric Errors Using the Laser Ball Bar," ASPE Proceedings vol. 10, pp. 76-79, 1994.

- Ziegert, J., Kalle, P., "Error Compensation in Machine Tools, a Neural Network Approach," *Journal of Intelligent Manufacturing*, vol. 5, pp. 143-151, 1994.
- Zhang, G., Veale, R., Charlton, T., Bochart, B., Hocken, R., "Parametric Error Measurement and Compensation on a CMM," *CIRP Annals*, 34/1 pp. 445-448, 1985.

BIOGRAPHICAL SKETCH

The author was born April 16, 1965, in Atlanta, Georgia, to Charles and Carol Mize. He graduated from Auburn University in 1987 with a bachelor's degree in mechanical engineering. Following graduation he began work at Pratt & Whitney Aircraft as a design engineer until 1991. From there he enrolled at the University of Florida, obtaining a master's degree in mechanical engineering in 1993. After graduation he started an engineering company with Dr. John Ziegert to promote the use of the laser ball bar. Simultaneously he pursued his Doctor of Philosophy degree in mechanical Engineering at the University of Florida.

I certify that I have read this study and that in my opinion it conforms to acceptable standards of scholarly presentation and is fully adequate, in scope and quality, as a dissertation for the degree of Doctor of Philosophy.



Kevin S. Smith, Chair
Associate Professor of Mechanical
Engineering

I certify that I have read this study and that in my opinion it conforms to acceptable standards of scholarly presentation and is fully adequate, in scope and quality, as a dissertation for the degree of Doctor of Philosophy.



Jiri Tlustý
Graduate Research Professor of
Mechanical Engineering

I certify that I have read this study and that in my opinion it conforms to acceptable standards of scholarly presentation and is fully adequate, in scope and quality, as a dissertation for the degree of Doctor of Philosophy.



John K. Schueller
Associate Professor of Mechanical
Engineering

I certify that I have read this study and that in my opinion it conforms to acceptable standards of scholarly presentation and is fully adequate, in scope and quality, as a dissertation for the degree of Doctor of Philosophy.



Ashok V. Kumar
Assistant Professor of Mechanical
Engineering

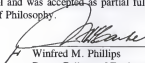
I certify that I have read this study and that in my opinion it conforms to acceptable standards of scholarly presentation and is fully adequate, in scope and quality, as a dissertation for the degree of Doctor of Philosophy.



Ramakant Srivastava
Professor of Electrical and Computer
Engineering

This dissertation was submitted to the Graduate Faculty of the College of Engineering and to the Graduate School and was accepted as partial fulfillment of the requirements for the degree of Doctor of Philosophy.

August, 1998



Winfred M. Phillips
Dean, College of Engineering

Karen A. Holbrook
Dean, Graduate School

LD
1780
1998
.M6845

